THE EFFECT OF ADDED CO-SOLVENT ON THE PHASE BEHAVIOUR OF THE MICELLAR LIQUID CRYSTAL SYSTEM CAESIUM PENTADECAFLUOROOCTANOATE / WATER.

A thesis presented in partial fulfilment of the requirements for the degree of

Master of Science in Chemistry at Massey University.

Scott Jonathan Thomsen

1994

Acknowledgements.

My sincere thanks go to my supervisor, Associate Professor Ken Jolley for his encouragement, guidance, and patience.

My thanks also go to Dr Ashok Parbhu for his invaluable contribution to this work.

Special thanks go to my parents, Neville and Jennifer Thomsen, Elsthorpe.

Abstract

The effect of the addition of the co-solvents formamide (FA), *N*-methylformamide (NMF), *N,N*-dimethylformamide (DMF), and *N,N*-dimethylacetamide (DMA) on the phase behaviour of the micellar liquid crystal system caesium pentadecafluorooctanoate (CsPFO)/D_2O (weight fraction CsPFO=0.5) has been determined. In all cases the effect of the addition of co-solvent is to decrease the isotropic (I)-to-nematic (N_D^+) and the nematic - to - lamellar (L_D) phase transition temperatures. At a co-solvent mole fraction of 0.01 the observed decreases in the I-to-N_D^+ phase transition temperatures (T_{NI}) were 5.3 K, 15.5 K, 15.7 K, and 18.8 K for the co-solvents FA, NMF, DMF, and DMA respectively, whilst the corresponding decrease for the N_D^+-to-L_D phase transition temperatures (T_{NL}) were 5.5 K, 16.1 K, 16.3 K, and 19.1 K. Thus, at low co-solvent concentrations, the main effect is simply to displace the phase transition lines to lower temperatures and there is no significant change in the overall phase behaviour other than a small increase in the temperature range of the N_D^+ phase. ^2H NMR measurements reveal that, in all cases, increasing the co-solvent concentration at constant temperature results in concomitant decreases in micelle aggregation numbers but the micelle sizes at T_{NI} and those at T_{LN} are essentially the same, i.e. the phase transitions are determined by hard particle interactions. Thus, the effect of co-solvent on the phase behaviour can be understood in terms of changes in micelle self-assembly, with addition of co-solvent shifting the distribution of micelle sizes to a lower mean aggregation number and decrease in temperature shifting the distribution of micelle sizes to a higher one. NMF, DMF, and DMA have a much greater effect on micelle size distribution than does FA.

Table of Contents.

1. Introduction.

Short chain perfluorocarbon carboxylic acids are exceptional for their preference to form solutions of discotic micelles which are stable over wide concentration and temperature intervals. This results in generic phase behaviour[1-3] in which the discotic micelles, with increasing concentration, undergo a sequence of disorder-order transitions to form first a nematic phase and, subsequently, a smectic lamellar phase[4,5] The nematic phase N_D^+ is characterised by long-range correlations in the orientation of the symmetry axes of the micelles, whilst in the dilute lamellar phase L_D the micelles are arranged on equidistant planes.

The origin of the stability of discotic micelles is not currently understood, indeed simple statistical mechanical models suggest that they are intrinsically unstable and should undergo spontaneous growth to form infinite bilayers as is the case for phospholipids for example[6]. The existence of discotic micelles is now universally excepted, however, and theoretical models have been proposed to account for their intrinsic stability. Within the framework of the McMullen model[7,8], the micelle is taken to be an oblate right-circular cylinder (body) closed by a half-toroidal rim. The chemical potential of a surfactant molecule will clearly be different in the "body" than in the "rim". It has been shown that only small discotic micelles can be stable, and this requires that the chemical potential of the surfactant in the rim be slightly greater than in the body so that the entropy of mixing off-sets their explosive growth into infinite bilayers.

Discotic nematic phases are found intermediate to isotropic micellar solutions at high temperatures/low concentrations and a smectic (lamellar) phase at lower temperatures/higher concentrations. They appear to be stable within the concentration interval about 0.1 to 0.5 volume fraction of amphiphile. Across this concentration interval the axial ratio a/b, where a is the length of the major, or symmetry axis and b the length of the two equivalent minor perpendicular axes, is typically in the range 0.25 to 0.5 for disc-shaped micelles and the maximum dimension of the micelle is of the order of the separation of the centres-of-mass. Thus, an Onsager type[9] description of the nematic order seems appropriate. For flat discs of depth d and diameter σ the volume fractions in the co-existing isotropic and nematic phases are: ϕ_i=2.97d/σ and ϕ_n=3.20d/σ[10,11]. For particles with smaller anisotropies computer simulations[12-14]of hard ellipsoids have established that nematic states exist from a/b < 1/2.75 for oblate ellipsoids. Theoretical treatments[15] have established the relation between $\phi_{i,n}$ and a/b for these small ellipsoids making comparison with experiment practicable: for oblate ellipsoids with a/b =1/5, ϕ_i = 1.67a/b and ϕ_n = 1.80a/b. Computer simulations on cut spheres[16] defined by a length-to-width ratio L/D, where D is the sphere diameter and L

($<D$) is the distance between the parallel flat surfaces, reveal a transition from a nematic phase to a translationally ordered columnar phase at higher densities for $L/D = 0.1$. However, the inherent distribution in size of the aggregates in micellar nematic phases is expected to significantly affect the structure of any translationally ordered phases which occur[17]. The micelle sizes are expected to vary with concentration and temperature and to depend upon the nature of the forces between the micelles and also upon any coupling to the symmetry and order of the mesophase. This will have a marked effect on the phase behaviour. Thus, any theory of micellar nematic phases must include the self-assembly behaviour of surfactants in aqueous solution. Taylor and Herzfeld[18] have considered liquid crystal phases formed in reversibly self-assembling systems (micellar liquid crystals) within the framework of a hard-particle model. The discotic system consists of a set of reversibly assembled polydisperse right cylindrical discs. The monomer unit was a symmetric right cylinder and a free energy of association of $-\phi(T)k_BT$ was assigned to each monomer-monomer contact. Using a scaled particle treatment of fluid configurational entropy and a cell description of periodic columnar density modulation they obtained a phase diagram which has many features in common with the experimental phase diagram for the CsPFO/water[1,2,19] and APFO/water[3] systems. In particular the inclusion of polydispersity in the model is sufficient to suppress columnar ordering[17] and favoured a translationally ordered smectic phase at high particle volume fractions. The volume fraction dependence of the orientational order parameters and average disc axial ratios were also calculated for a series of temperatures (ϕ^{-1}) chosen so that the values of these parameters at the phase transitions could be obtained and tested against experiment.

It has been shown that the addition of the co-surfactant perfluorooctanol to the CsPFO/H_2O system leads to larger micelles[20]. The long chain surfactant molecules form part of the micelles and lead to a reduction in the electrostatic repulsion between the carboxylate head groups. The addition of electrolyte also leads to larger micelles[21,22] by influencing the self assembly of the surfactant molecules.

The object of this study is to determine the phase behaviour for the CsPFO/D_2O system upon the addition of the four co-solvents formamide (FA), *N*-methylformamide (NMF), *N,N*-dimethylformamide (DMF), and *N,N*-dimethylacetamide (DMA) using ^2H and ^{133}Cs NMR spectroscopy to determine the phase transition temperatures. The phase behaviour of these systems will be compared to that of the binary CsPFO/D_2O system[1] to examine how the co-solvent effects the phase behaviour in terms of the self assembly of the discotic micelles. It is well known that the simple amides FA, NMF, DMF and DMA are of interest as model compounds in biochemistry. They are of interest here because they represent, in the given sequence, a transition from a small, hydrogen-bonding, protic solvent with no hydrophobic groups (FA) to a large, aprotic

solvent with three methyl groups (DMA). The number of methyl groups in a molecule is known to strongly affect structural and dynamic properties of aqueous mixtures of these molecules. The range they exhibit in their physical properties (such as relative permittivity and surface tension) is of particular interest.

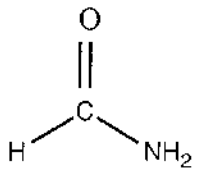

FORMAMIDE

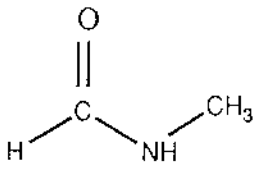

N-METHYL FORMAMIDE

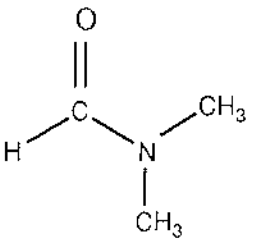

N,N-DIMETHYL FORMAMIDE

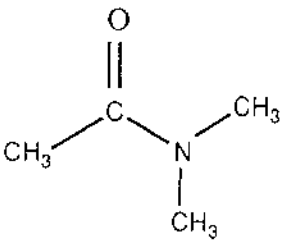

N,N-DIMETHYL ACETAMIDE

In all the experiments the CsPFO to D_2O ratio is kept constant and small amounts of co-solvent are added such that the phase behaviour of the binary CsPFO/D_2O system is essentially preserved. It will be shown that the mechanism for the phase transitions is essentially a hard particle one and it is the self assembly which determines the phase behaviour.

2.Experimental.

2.1 Chemicals.

N,N-dimethyl formamide and N,N-dimethyl acetamide (BDH AnalaR grade) were dried over calcium hydride and distilled under vacuum. N-methyl formamide (Aldrich) was of the highest purity available (99%) and used without further purification. Formamide (BDH AnalaR grade) was dried over anhydrous sodium sulphate and distilled under vacuum. N,N-dimethyl formamide-*d7* (99.5 atom % D) and deuterium oxide (99.9 atom % D) (both from Aldrich) were used without further purification. The above solvents are all hygroscopic hence were stored under dry nitrogen in a dessicator.

Caesium pentadecafluorooctanoate (CsPFO) was made by neutralising the sparingly soluble parent acid (Aldrich) with caesium carbonate (Reidel-de Haen) in deionized and doubly distilled water. The slightly alkaline solution was tested with litmus paper (BDH) then freeze-dried. The pure CsPFO salt was obtained by double recrystallisation from 50% butanol/hexane. Residual solvent was removed by prolonged heating (at least 24 hours at 50 °C) under vacuum. The pure crystals appeared waxy and pure white. CsPFO is hygroscopic so was also kept in a dessicator.

A hazard sheet for handling these chemicals is included in Appendix 2

2.2 Sample Preparation.

2.2.1 NMR Sample Preparation.;

Samples were prepared to give a constant CsPFO to D_2O mass ratio with varying amount of amide in the following way. Stock solutions of CsPFO in D_2O were gravimetrically prepared using a Mettler AT 261 Delta Range five-figure balance. CsPFO was added by funnel to a 10 ml ampoule. The mass of D_2O required to make up the desired salt mass fraction (w=0.4 or 0.5) was calculated and added by long hypodermic syringe. The ampoule was flame sealed and the solution thoroughly mixed. Care was taken not to contaminate the ampoule neck during weighing to prevent evaporation of D_2O or decomposition of salt during sealing. Samples prepared in this manner varied in composition to within $\pm$ 0.002 mass fraction.

The stock solution was heated into the isotropic phase and thoroughly mixed. A sample was prepared by first adding a 0.6 ml aliquot of the stock solution by syringe into a preweighed 5 mm o.d. NMR tube that had been cleaned with concentrated nitric acid, thoroughly washed with deionized doubly distilled water and dried in an oven at

80 °C. The mass of stock solution in the NMR tube was then determined and this was used to calculate the approximate volume of amide required. The amide was added to the NMR tube in a fume cupboard using a glass syringe. The stoppered solutions were reweighed then flame sealed. During the course of the work presented here it was necessary to prepare several stock CsPFO/D_2O solutions. A control sample (no amide added) was thus retained from every batch and the I-to-N_D^+ phase transition temperature determined to ensure uniform stock solution concentration. Thorough mixing of the samples in the isotropic phase was performed prior to use.

2.2.2 Conductivity Sample Preparation.

Stock D_2O/amide solvent solutions were gravimetrically prepared in 25 cm^3 volumetric flasks (in a fume cupboard) such that the mole fraction of amide in D_2O was 0.0231 (corresponding to approximately 5% by mass formamide in D_2O). Standard solutions of approximately 0.1 mol kg^{-1} CsPFO in these solvents were made up in 10 cm^3 volumetric flasks. After the conductivity of a solution had been measured, most of the analyte was recovered and reweighed. This was then diluted by a known mass of solvent and the new amphiphile concentration calculated. This process was repeated until the CMC had been defined.

2.3 Instrumentation.

2.3.1 Temperature control.

Precise, stable and accurate temperature control is fundamental to the determination of phase transition temperatures. It will be seen that both ^2H and ^{133}Cs quadrupole splittings are strongly temperature dependent. The JEOL JNM-GX270 NMR spectrometer is supplied with an air flow temperature control system. The use of air, with its low heat capacity, only allows temperatures stable to ± 0.1 K and gives rise to thermal gradients along the sample. This leads to sample inhomogeneity through solvent distillation and phase separation which manifests itself as a broadening of NMR spectrum lines. A double-pass water flow sample cell has been developed[23] (and recently modified) (figure 2.1) which, when coupled to a Colora WK3 cryostat gives temperature control to within ± 5 mK over several hours and which has been shown to produce samples with exceptional temperature and concentration homogeneity.

Figure 2.1 Double-pass water flow sample cell used to control the sample temperature during NMR experiments using a JEOL GX270 spectrometer. The Teflon rotor is the standard 10 mm sample spinner supplied by the spectrometer manufacturer. The water is pumped to the cell by a Colora WK3 cryostat.

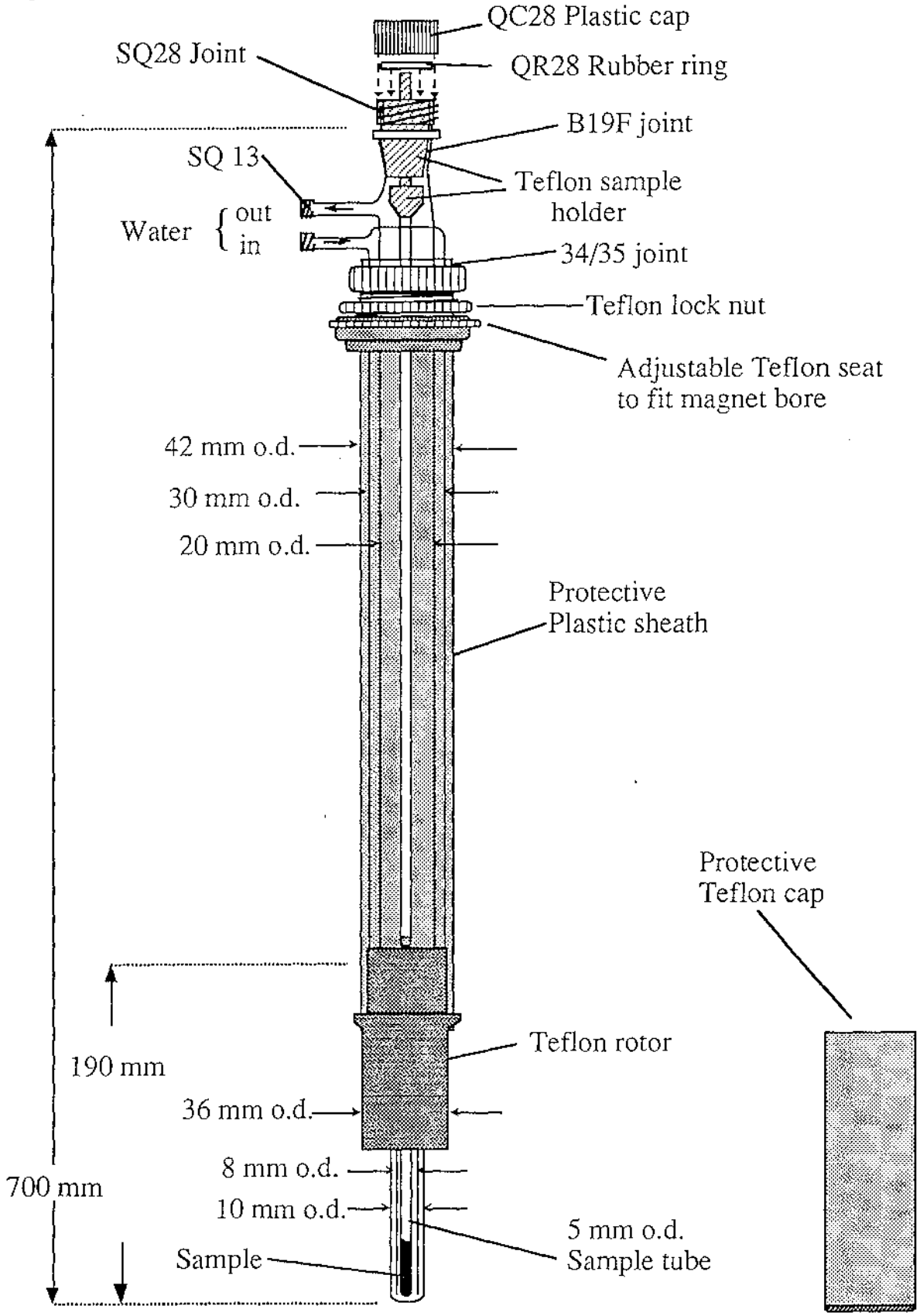

Temperature control during conductivity measurements is also important so a double-pass water flow cell (figure 2.2) was designed and temperature control achieved by using a Colora WK3 cryostat as for the NMR experiments.

Figure 2.2 Double-pass water flow sample cell used to control the sample temperature during conductivity experiments. The water is pumped to the cell by a Colora WK3 cryostat.

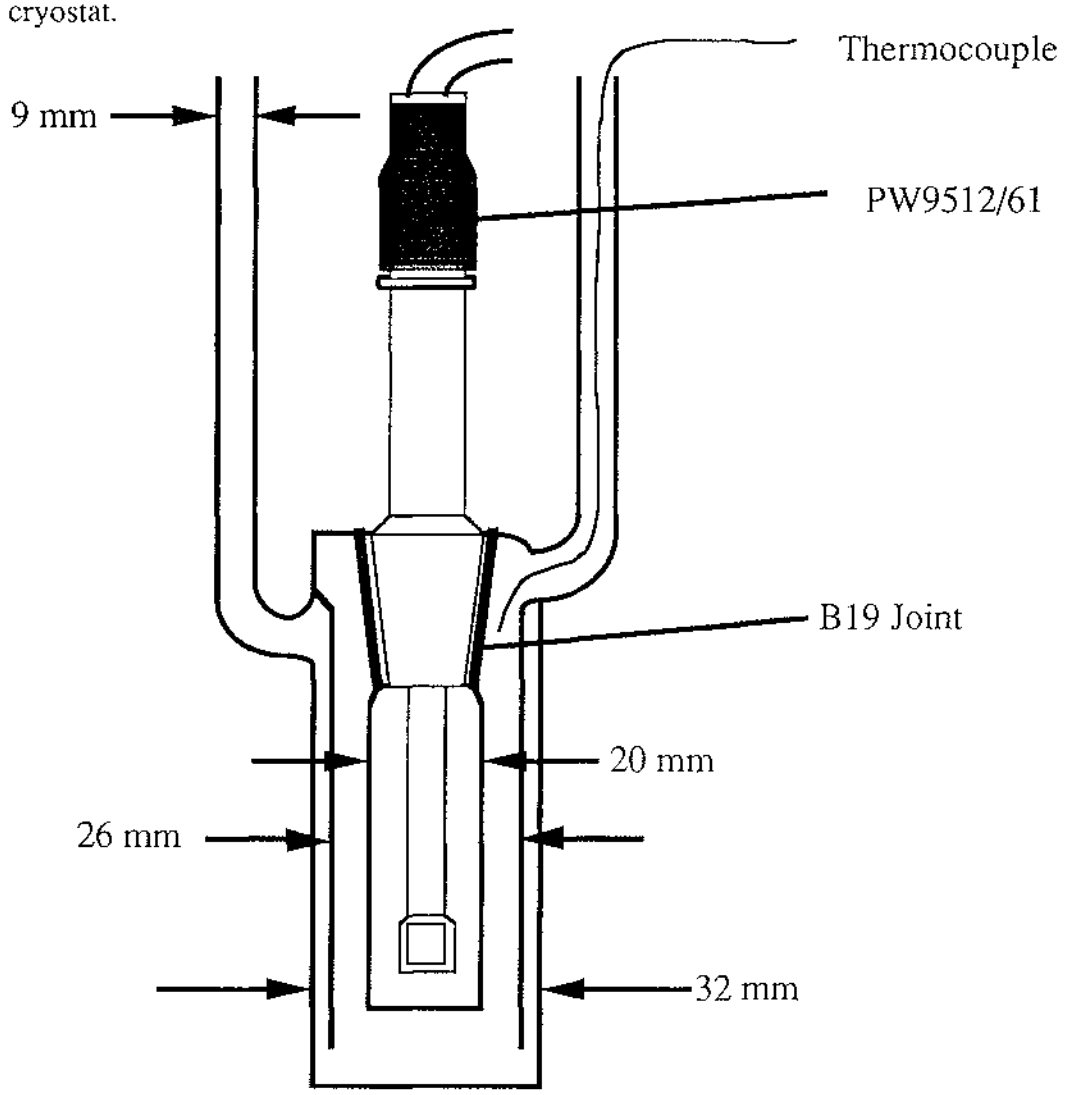

2.3.2 Temperature Measurement.

Temperature was continuously monitored during both the NMR and conductivity measurements by the insertion of a copper/constantin thermocouple into the water flow close to the sample. The potential between this and a reference thermocouple maintained at 0 °C by immersion in an ice slurry was measured to an accuracy of 0.1 μV using a Philips PM2535 systems multimeter. The thermocouple had been calibrated at 2 K intervals to an accuracy and precision of ±1 mK against a

Hewlett-Packard 2804A digital quartz thermometer with a 2805A temperature probe. The potential was converted to temperature by linear interpolation between calibration points using a program written on MathCAD.

2.3.3 NMR Instrumentation.

A JEOL JNM-GX270 spectrometer with an Oxford Instruments 6.34 Tesla wide bore superconducting magnet was used to observe ^{2}H and ^{133}Cs nuclei using an NM-G2710 10mm tuneable probe.

The probe was tuned to the ^{133}Cs frequency giving a $\pi/2$ pulse width of 19 μs and a consequent effective spectral freqency range of about 50 kHz. A typical ^{133}Cs spectral frequency range was 30 kHz. ^{2}H spectra were recorded without retuning the probe so that consecutive ^{133}Cs and ^{2}H spectra could be obtained without delay. The ^{2}H $\pi/2$ pulse when the probe was tuned to the ^{133}Cs frequency was 400 μs and a $\pi/4$ pulse of 200 μs was used for spectral accumulation, giving an effective spectral range of about 5 kHz. This spectral range was more than adequate for all ^{2}H spectra where typical quadrupole splittings ranged from 200 Hz to 1 kHz. For the ^{133}Cs counterion measurements and the ^{2}H NMR of heavy water the FID was collected immediately following a $\pi/2$ pulse.

Typical acquisition parameters are shown in table 2.1.

Table 2.1. Typical NMR acquisition parameters.

Nucleus	^{2}H	^{133}Cs
Experiment Mode	Single Pulse-Non decoupled	Single Pulse-Non decoupled
Observation Frequency	41.47 MHz	35.31 MHz
Sweep Width	2 kHz	10-60 kHz
Data Points	8192	32768
Broadening Factor	0.1 Hz	1 Hz
Accumulations	4	16
Pulse Width	200 μs	19 μs
Pulse Delay	2 s	0.5 s

2.3.4 Conductivity Instrumentation.

The cell constant of a Philips PW9512/61 conductivity cell was determined at 298 K using a standard 0.100 mol l^{-1} KCl solution and found to be 0.725 cm^{-1}. This cell, attached to a Philips PW9509 digital conductivity meter, was then used to measure conductivities of samples at a measuring frequency of 2000 Hz, the highest frequency available on the PW9509 meter.

3. NMR Theory.

The sensitivity and selectivity of NMR make it a very useful experimental technique on both a macroscopic and molecular level. Quadrupole splittings of nuclei in anisotropic media such as lyotropic liquid crystals are very sensitive to changes in sample composition and temperature, qualities that are ideal for establishment of phase diagrams.

Not only are quadrupole splittings characteristic of a particular phase but are also a function of the size and shape of micellar aggregates, the orientational order parameter of the micelle, and the fraction of bound species. The contribution of these factors to the quadrupole splittings will be presented in the following discussion. ^{133}Cs chemical shift anisotropy will also be discussed.

The magnitude of the spin angular momentum vector **P** for any nucleus is given by

$$P = \hbar\sqrt{I(I+1)}$$

where I is the nuclear spin quantum number. The direction of **P** is described by m_I, the spin angular momentum number along the z-axis such that

$$P_z = \hbar m_I$$

where m_I possesses 2I+1 values (+I, +I-1, ...-I).

By virtue of their charge, all nuclei possess a magnetic moment μ, which is related to **P** by the nuclear magnetogyric ratio γ, a property intrinsic to a particular nucleus, i.e.

$$\mu = \gamma \mathbf{P}.$$

Thus,

$$\mu_z = \gamma \hbar m_I.$$

In the absence of an external magnetic field nuclear spin states are degenerate. Under the influence of a magnetic field **B**, the degeneracy is lifted and the nuclei possess discrete energy values given by

$$\mathbf{E} = -\mu.\mathbf{B}$$

with components in the external field direction of

$$E_z = -\mu_z B = -\gamma\hbar m_I B.$$

The selection rule governing transitions between the 2I+1 energy states separated by $|\gamma\hbar B|$ is $\Delta m_I = \pm 1$. Thus, transitions may be induced by the application of oscillating electromagnetic fields with energy

$$\Delta E = h\nu = \gamma\hbar B$$

where ΔE is the Zeeman energy. In the absence of perturbations, such as chemical shifts and scalar couplings, identical nuclei would absorb at the same frequency, the Lamor precessional frequency, given by

$$\nu = \frac{\gamma}{2\pi} B.$$

Absorption frequencies of identical nuclei are (fortunately) modified by the electronic environment around them. Heisenberg's uncertainty principle, relaxation effects and inhomogeneities in the magnetic field cause absorption lines to have finite widths[24].

3.1 Quadrupole Energies For Nuclei With $I > \frac{1}{2}$

Nuclei with $I > \frac{1}{2}$ have an ellipsoidal charge distribution and hence possess a quadrupole moment. Under the influence of an electric field, the quadrupole nucleus will minimize electrostatic energy by adopting favoured alignments. This is illustrated in figure 3.1.

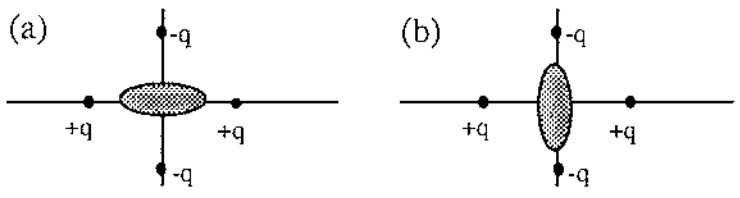

Figure 3.1 A nucleus with ellipsoidal charge distribution in a field of four charges. Position (b) is more energetically favourable than (a).

As a consequence of this coupling of the quadrupole moment with the electric field gradient, the degeneracy of the Zeeman energy levels is lifted to give 2I transitions with a first order intensity distribution [I(I+1)-m(m+1)][25]. The magnitude of the coupling is a function of the nuclear quadrupole - electric field gradient constant χ. For

the nuclei considered in this thesis (^{2}H and ^{133}Cs), χ is negligibly small compared to the nuclear Zeeman energy hence all spectra are first order. The energy levels are given by[24]

$$E_{m_I} = \gamma\hbar m_I B + \frac{3m_I^2 - I(I+1)}{4I(2I-1)} hq_{zz}$$

where q_{zz} is the component of the nuclear quadrupole - electric field gradient interaction tensor parallel to the magnetic field. Figure 3.1 shows an energy level diagram for ^{133}Cs ($I=\frac{7}{2}$).

As a consequence of the positive diamagnetism of CsPFO/^2H_2O in the nematic phase, the nematic director **n** undergoes spontaneous alignment with the magnetic field **B**. Nuclei with $I>\frac{1}{2}$ in a macroscopically aligned uniaxial mesophase will give a first order spectrum consisting of 2I equally spaced lines with separation[26,27]

$$\Delta\tilde{\nu}(\phi) = \frac{3}{2I(2I-1)}\left|\tilde{q}_{zz}\right| P_2(\cos\phi) \qquad 3.1$$

termed the quadrupole splitting. The upper tilde denotes a partially averaged quantity. $P_2(\cos\phi) = \frac{1}{2}\left(3\cos^2\phi - 1\right)$is a second-rank Legende polynomial and is a function of ϕ, the angle between the mesophase director and the spectrometer magnetic field **B**.

For a uniaxial macroscopically aligned diamagnetically positive mesophase **n** and **B** are collinear and $P_2(\cos\phi) = 1$. Thus in all experiments carried out on the GX270 equation 3.1 reduces to[27]

$$\Delta\tilde{\nu}(\phi=0) = \frac{3}{2I(2I-1)}\left|\tilde{q}_{zz}\right| \qquad 3.2$$

Here, $\left|\tilde{q}_{zz}\right|$ is the partially averaged component of the nuclear quadrupole electric field gradient interaction tensor measured parallel to **n** and is given by

$$\left|\tilde{q}_{zz}\right| = \sum_n p_n \chi_n \left[S_{cc}^n + \frac{1}{3}\eta_n (S_{aa}^n - S_{bb}^n)\right]$$

where S_{ij} are the elements of the Saupe[28] ordering matrix for the principle axes (a,b,c) of the nuclear quadrupole interaction tensor at the n'th site which has statistical weight p_n, $\chi_n = \left(e^2 qQ/h\right)_n$ is the corresponding quadrupole coupling constant, and η_n is the asymmetry parameter for the electric field gradient tensor at the site defined as $\eta = \left(q_{aa} - q_{bb}\right)/q_{cc}$ where q_{ii} are the components of the electric field gradient tensor. For a uniaxial mesophase, the asymmetry parameter is zero since $q_{aa} = q_{bb}$.

Figure 3.1 The energy level diagram for an $I=\frac{7}{2}$ nucleus (^{133}Cs) showing the effect of a first order quadrupolar interaction on the Zeeman energies.

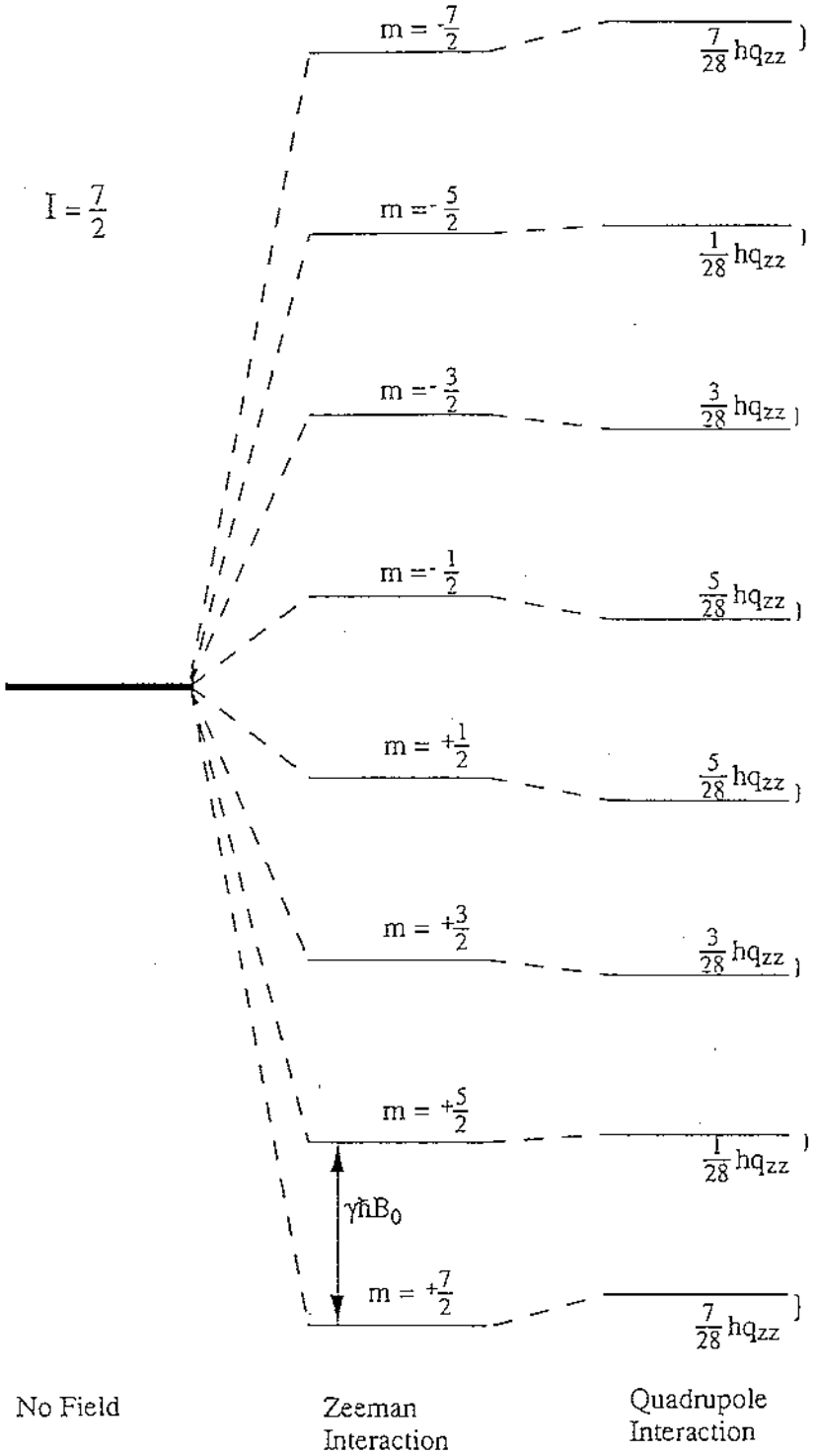

p_n, χ_n, and η_n will vary from site to site i.e. they are determined by the detailed structure of the micelle.

In order to separate contributions to the quadrupole splitting that arise from micellar and orientational order parameter fluctuations, it has been shown[1] that equation 3.2 can be rewritten as

$$\Delta\tilde{\nu}=\frac{3}{2I(2I-1)}\left|\tilde{q}_{zz}\right|_S S \qquad 3.3$$

where $\left|\tilde{q}_{zz}\right|_S$ is now solely determined by the solution concentration and the detailed aggregate structure and S is an order parameter which represents an average of the orientations of the micellar axes with respect to **n**. S accounts for oscillations of the local director **n** about the macroscopic director (collinear with **B**), and fluctuations in the micellar symmetry axis **m** about **n** (figure 3.3).

Figure 3.3

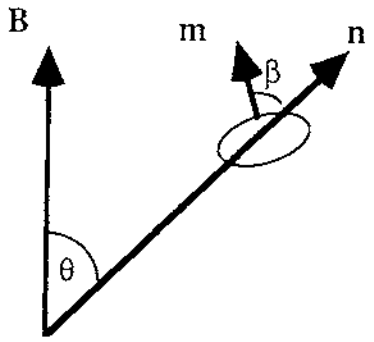

S may be expressed

$$S = \left\langle P_2(\cos\theta)\right\rangle\left\langle P_2(\cos\beta)\right\rangle = P_{2n}P_{2m}.$$

P_{2n} and P_{2m} represent fluctuations of the local director and the micelle respectively. The angular brackets denote an ensemble average. S=1 for a perfectly aligned sample and S=0 for a completely disordered (isotropic) phase.

Specific expressions for $\left|\tilde{q}_{zz}\right|_S$ for ^2H and ^{133}Cs nuclei are presented in the next section.

3.1.1 ^2H (I=1)

For a ^2H nucleus in heavy water equation 3.3 becomes

$$\Delta\tilde{\nu}=\frac{3}{2}\left|\tilde{q}_{zz}\right|_S S \qquad 3.4$$

where

$$\left|\tilde{q}_{zz}\right|_S = \left\langle P_2(\cos\alpha)\right\rangle_S \chi_D \frac{x_A}{x_W} n_b S_{OD}. \qquad 3.5$$

$\left\langle P_2(\cos\alpha)\right\rangle_S \left(=\left\langle\frac{3}{2}\cos^2\alpha-\frac{1}{2}\right\rangle_S\right)$ accounts for the motional averaging of contributions from ^2H_2O at sites over the micelle surface, and is a function of α, the angle between

the normal to the micelle surface and the micelle symmetry axis. χ_D is the quadrupole coupling constant for ^2H in heavy water (assumed equivalent for all sites), x_A and x_W are the mole fractions of amphiphile and water respectively, n_b is the number of water molecules bound per molecule of amphiphile, and S_{OD} is an order parameter representing averaging due to local reorientation of bound water. For water molecules not bound to the surface $|\tilde{q}_{zz}|_S = 0$.

3.1.2 ^{133}Cs ($I=\frac{7}{2}$)

For a $^{133}Cs^+$ ion equation 3.3 becomes

$$\Delta\tilde{\nu}=\frac{1}{14}|\tilde{q}_{zz}|_S S \qquad 3.6$$

where

$$|\tilde{q}_{zz}|_S = \langle P_2(\cos\alpha)\rangle_S \chi_{Cs}\beta_{Cs} \qquad 3.7$$

where χ_{Cs} is the quadrupole coupling constant of the ^{133}Cs nucleus and β_{Cs} is the fraction of caesium ions bound to the micelle. For ^{133}Cs nuclei not bound to the surface $|\tilde{q}_{zz}|_S = 0$, so that the observation of a finite quadrupole splitting implies that for the fraction of bound ions the hydration shell must be distorted from spherical symmetry[2].

3.2 ^{133}Cs Chemical Shift Anisotropies.

The large ^{133}Cs chemical shift range makes it possible to observe, in anisotropic liquid crystalline phases, both the isotropic and anisotropic contributions to the chemical shift. In an isotropic liquid rapid molecular motion averages out the anisotropic component. In an ordered phase the anisotropic component always dominates and is revealed in the -1/2 to +1/2 Zeeman transition which, to first order, contains no contribution from quadrupole interactions. The chemical shift anisotropy may be used as an alternative to measuring quadrupole splittings as a method to track phase transitions. For a monodomain macroscopically aligned discotic micellar mesophase, the partially averaged chemical shift is given by[29]

$$\tilde{\sigma}_{zz}(\phi) = \sigma_i + \frac{2}{3}\sum p_n\left[S^n_{cc}\left\{\sigma^n_{cc} - \frac{1}{2}\left(\sigma^n_{aa} + \sigma^n_{bb}\right)\right\} + \frac{1}{3}\left(S^{n_n}_{aa} - S^n_{bb}\right)\left(\sigma^n_{aa} - \sigma^n_{bb}\right)\right]P_2(\cos\phi) \qquad 3.8$$

Averaging due to the microscopic motions of the Cs^+ ions reduces equation 3.8 to

$$\tilde{\sigma}_{zz}(\phi) = \sigma_i + \frac{2}{3}(\sigma_{\parallel} - \sigma_{\perp})_M S\left\langle P_2(\cos\alpha)\right\rangle_S \beta_{Cs} P_2(\cos\phi) \quad 3.9$$

where $(\sigma_{\parallel})_M$ and $(\sigma_{\perp})_M$ are the respective components of the axially symmetric chemical shift shielding tensor for bound counterions parallel and perpendicular to the micelle surface, and

$$\sigma_i = \frac{1}{3}\{Tr\sigma^b\}\beta + \sigma^f(1-\beta), \quad 3.10$$

with the superscripts denoting "bound" and "free" counterions.

The chemical shift in the isotropic phase or in a macroscopically aligned uniaxial phase with ϕ=54°44' is σ_i. In a macroscopically aligned phase in which ϕ=0°, the second term in equation 3.9 is non-zero. This gives rise to a discontinuity in the ^{133}Cs shift at the isotropic to nematic transition of magnitude

$$\tilde{\sigma}_{zz}(0°) - \sigma_i = \frac{2}{3}\Delta\tilde{\sigma} = \frac{2}{3}(\sigma_{\parallel} - \sigma_{\perp})_M S\left\langle P_2(\cos\alpha)\right\rangle_S \beta_{Cs} \quad 3.11$$

where

$$\Delta\tilde{\sigma} = \tilde{\sigma}_{zz}(0°) - \tilde{\sigma}_{zz}(90°). \quad 3.12$$

$\Delta\tilde{\sigma}$ may also be determined directly from the powder spectrum of an unoriented sample[30].

4. The Effect of Co-Solvent on Liquid Crystal Phase Behaviour.

The phase diagrams presented here were all constructed from the results of ^{2}H or ^{133}Cs NMR measurements. For convenience the phase diagrams are presented first (section 4.1) before explaining how they were obtained (section 4.2).

4.1 Phase Diagrams.

A partial phase diagram for the binary CsPFO/D_2O system[2] is presented in figure 4.1. It shows a discotic micellar N_D^+ phase intermediate to an isotropic micellar solution phase I and a discotic micellar L_D phase. The N_D^+ phase is quite extensive and is seen to be stable between the mass fractions w of 0.225 and 0.632 and temperatures of 285.29 and 351.23 K. The lamellar-nematic-tricritical point Tcp is fixed at w=0.43 with corresponding temperature of 304.8 K. The other singular points to note are the critical end point Cep [T=285.72 K, w=0.287] where the line of second order L_D to N_D^+ transitions intersect the solubility curve T_c, the $I/N_D^+/L_D$ triple point [T=351.23 K, w_I=0.626, w_N=0.632, w_L=0.64], and the $I/N_D^+/K$ triple point [T=285.29 K, w_I=0.221, w_N=0.225, w_K=1.0]. The existence of the lamellar-nematic tricritical point indicates that the I to N_D^+ to L_D sequence of transitions is analogous to the isotropic liquid to nematic to smectic A sequence observed for thermotropic calamitic liquid crystals. This suggests that the transition is a simple order-disorder one and does not involve any significant change in the structure of the micelles. In this chapter the effect of the addition of co-solvent on the phase behaviour of samples with fixed CsPFO:D_2O ratios will be presented. The systems are thus ternary ones and the phase behaviour of such systems can be complex. In this study only a minute region of the ternary phase space will be investigated, in that the mole fraction of co-solvent is always much less than that of D_2O.

Originally a w=0.4 CsPFO/D_2O sample was chosen to study the effect of adding co-solvent on the phase behaviour. This was because the N_D^+ phase covered an accessible temperature range and isotropic samples were easily prepared. For this sample on cooling from the isotropic phase into the nematic phase a first order phase transition occurs. The upper T_{IN} and lower T_{NI} boundaries to the N_D^+ phase co-existence region are 306.70 K and 306.51 K respectively. Upon further cooling a second order transition from nematic to lamellar occurs at T_{LN}=301.52 K i.e the w=0.4 sample is below Tcp, the lamellar-nematic-tricritical point. The partial phase diagram for the CsPFO/D_2O/DMF system at the fixed CsPFO:D_2O mass ratio of 2:3 is presented in figure 4.2.

Figure 4.1 Phase Diagram for the CsPFO/D_2O system. Nomenclature: I, isotropic micellar solution phase; N_D^+, discotic nematic phase with positive diamagnetic susceptibility anisotropy; L_D, discotic lamellar phase; K, crystal; Tcp, the lamellar-nematic tricritical point; Tp(I,N,K), the isotropic micellar solution-nematic-crystal triple point; Tp(I,N,L), the isotropic micellar solution-nematic-lamellar triple point; Cep, the critical end point.

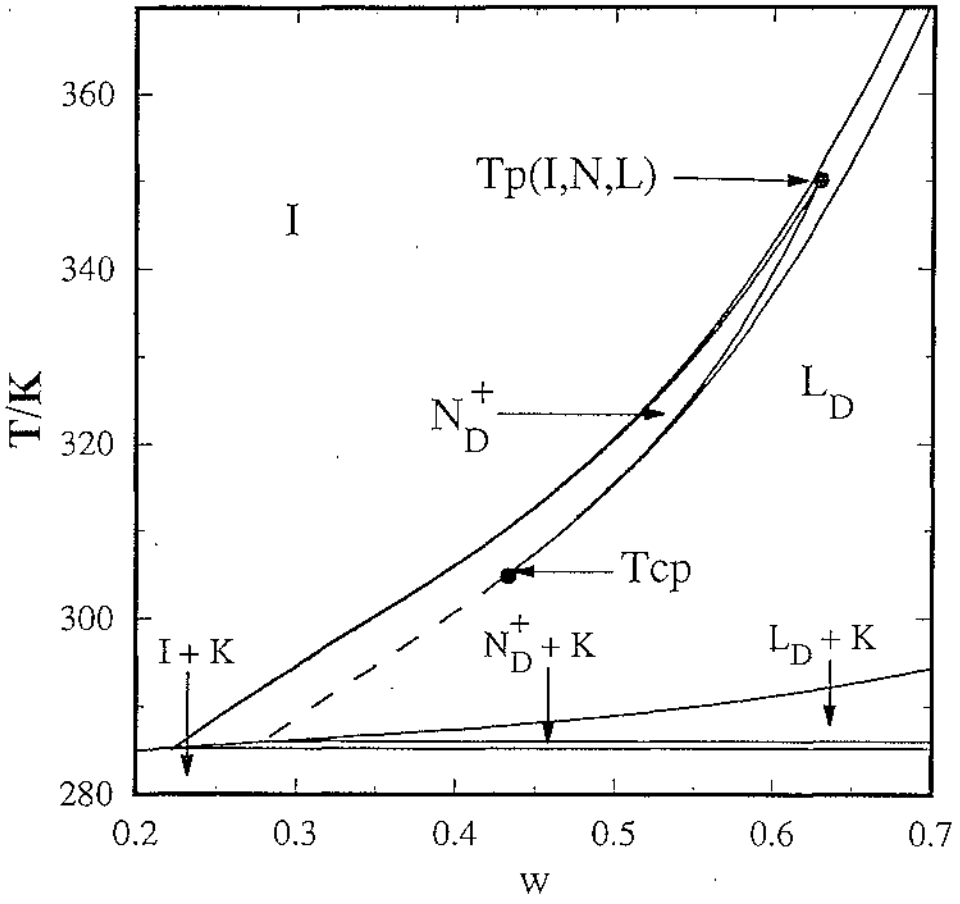

Figure 4.2 Partial Phase Diagram for the CsPFO/D_2O/DMF system showing the upper and lower boundaries to the isotropic solution/nematic (I/N_D^+) mixed phase region, and the N_D^+ to discotic lamellar L_D transition line. The ratio of CsPFO to D_2O is 2:3 by mass. The phase boundaries are degree three polynomials fitted to the experimental data points. The phase transition temperatures are tabulated in Appendix 1.

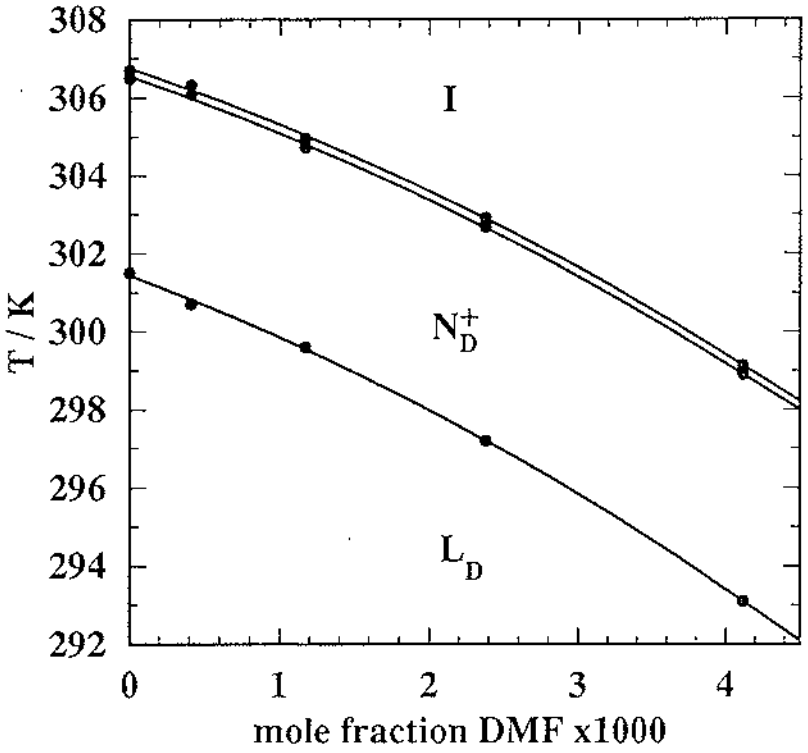

It is clear from figure 4.2 that adding DMF leaves the phase behaviour unchanged but depresses phase transition temperatures. This effect having been established, it was decided to shift the isopleth to the higher mass fraction of w=0.5 to expand the co-solvent concentration range that could be added while maintaining experimentally accessible phase transition temperatures. It is a creditable feature that the phase behaviour of the CsPFO/D_2O system has been so well defined to allow the choice of an appropriate mass fraction to suit a specific purpose. The phase behaviour along the 0.5 isopleth of figure 4.1 is different from that along the 0.4 isopleth only as far as the N_D^+ to L_D transition is concerned. For this sample on cooling from the isotropic phase into the nematic phase a first order phase transition occurs. The upper T_{IN} and lower T_{NI} boundaries to the I/N_D^+ phase co-existence region are 320.32 K and 319.82 K respectively. Upon further cooling from the nematic phase into the lamellar phase a first order phase transition occurs. The upper T_{NL} and lower T_{LN} boundaries to the N_D^+/L_D phase co-existence region are 315.18 K and 315.09 K respectively i.e. the w=0.5 sample is above Tcp. Partial phase diagrams for the CsPFO/D_2O/DMA, CsPFO/D_2O/DMF, CsPFO/D_2O/NMF and CsPFO/D_2O/FA systems at the fixed CsPFO:D_2O mass ratio of 1:1 are presented in figure 4.3. For clarity, only phase boundaries for the CsPFO/D_2O/FA, CsPFO/D_2O/DMF and CsPFO/D_2O/DMA systems are shown.

In all cases the overall phase behaviour of the pure CsPFO/D_2O system is essentially preserved when co-solvent is added, at least in the composition range studied here. The transitions remain either first or second order and the widths of the biphasic regions and nematic phase remain essentially constant irrespective of the concentration of the solvent (although there is a small increase in the width of the nematic phase at high DMF concentration in the w=0.5 CsPFO/D_2O mass fraction).

To first order then, the sole effect of the addition of co-solvent is to decrease the I-to-N_D^+ and the N_D^+-to-L_D+ phase transition temperatures. Furthermore, it is evident that at corresponding mole fractions addition of FA has less of an effect on the phase behaviour than NMF, DMF or DMA. The origin of this effect will be discussed in chapter 6.

Figure 4.3 Partial Phase Diagrams for the CsPFO/D_2O/DMA, CsPFO/D_2O/DMF, CsPFO/D_2O/NMF and CsPFO/D_2O/FA systems. For clarity, lines indicating the upper and lower boundaries to the isotropic solution/nematic (I/N_D^+) mixed phase region, and the N_D^+ to discotic lamellar L_D transition line are shown for the CsPFO/D_2O/DMA, CsPFO/D_2O/DMF and CsPFO/D_2O/FA systems only. The ratio of CsPFO to D_2O is 1:1 by mass. Phase boundaries are degree three polynomials fitted to the experimental data points. Also for clarity, only data points for T_{NI} and T_{LN} are shown. The phase transition temperatures are tabulated in Appendix 1.

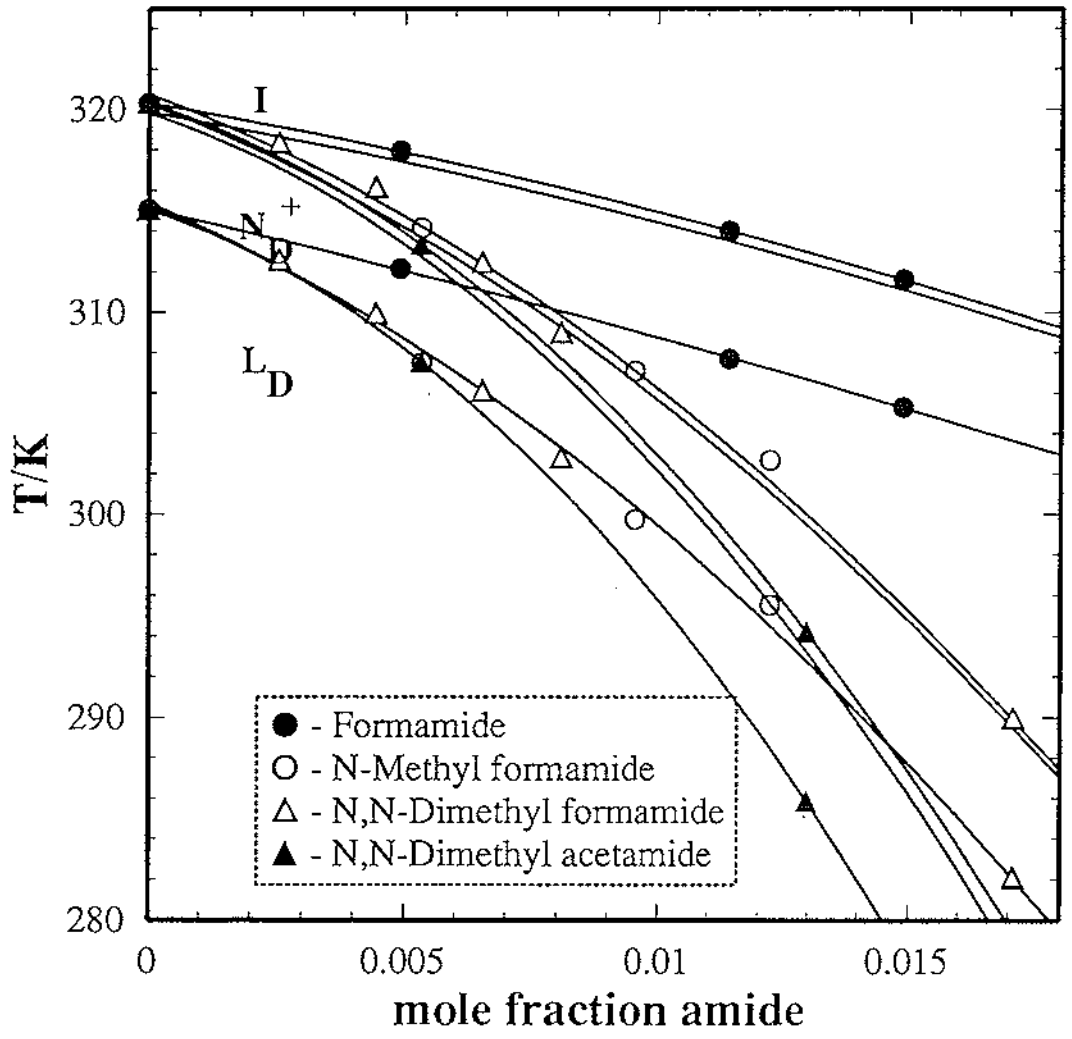

4.2. Phase Identification and Determination of Phase Transition Temperatures.

4.2.1 Phase Characterisation.

NMR measurements of the quadrupole splittings of ^2H in labelled water or of quadrupolar counterions, such as ^{133}Cs, is unparalleled as an experimental method for mapping phase diagrams and, in particular, for characterizing phase transitions. This is because the quadrupole splitting is a characteristic signature of a mesophase and is also a function of composition and temperature. It can therefore provide detailed information about the uniformity of composition and temperature in bulk samples and it can also be used to monitor the orientational distribution of the mesophase director and to distinguish between uniaxial and biaxial mesophases[31].

4.2.1.1 ^2H NMR Spectra.

The appearance of typical ^2H spectra are shown in figure 4.2.1. In an isotropic micellar solution phase only the Zeeman interaction is observed (figure 4.2.1a) since the order parameter S=0 (equation 3.4).

In the nematic phase (figure 4.2.1b) micelles exhibit macroscopic alignment with the magnetic field and $0<S<1$. Hence the ^2H spectrum here is a symmetric doublet with the quadrupole splittings given by equation 3.4. In a lamellar phase macroscopically aligned with the magnetic field, the ^2H spectrum is also a doublet, but with quadrupole splittings greater in magnitude. The two phases may be distinguished by the nature of the response of the mesophase director to changes in the orientation of the sample with respect to the spectrometer magnetic field[1]. If a sample in the lamellar phase is cooled outside the magnetic field an unoriented lamellar phase is obtained, i.e. there is a random distribution of local directors. Since the lamellar phase has an infinite rotational viscosity coefficient it will not reorient when replaced inside the magnet. The ^2H spectrum of an unoriented sample consists of a Pake doublet (figure 4.2.1c) where the central doublet represents singularities at $\phi=90°$ and the outer doublet, those at $\phi=0°$. The separation of the latter is given by equation 3.4.

Figure 4.2.1 ^2H NMR spectra for a macroscopically aligned w=0.5 CsPFO/^2H_2O sample obtained by cooling from the isotropic (a) into the nematic phase (b). Spectrum (c) is for an unoriented lamellar phase produced by cooling the sample from the isotropic into the lamellar phase outside the magnetic field.

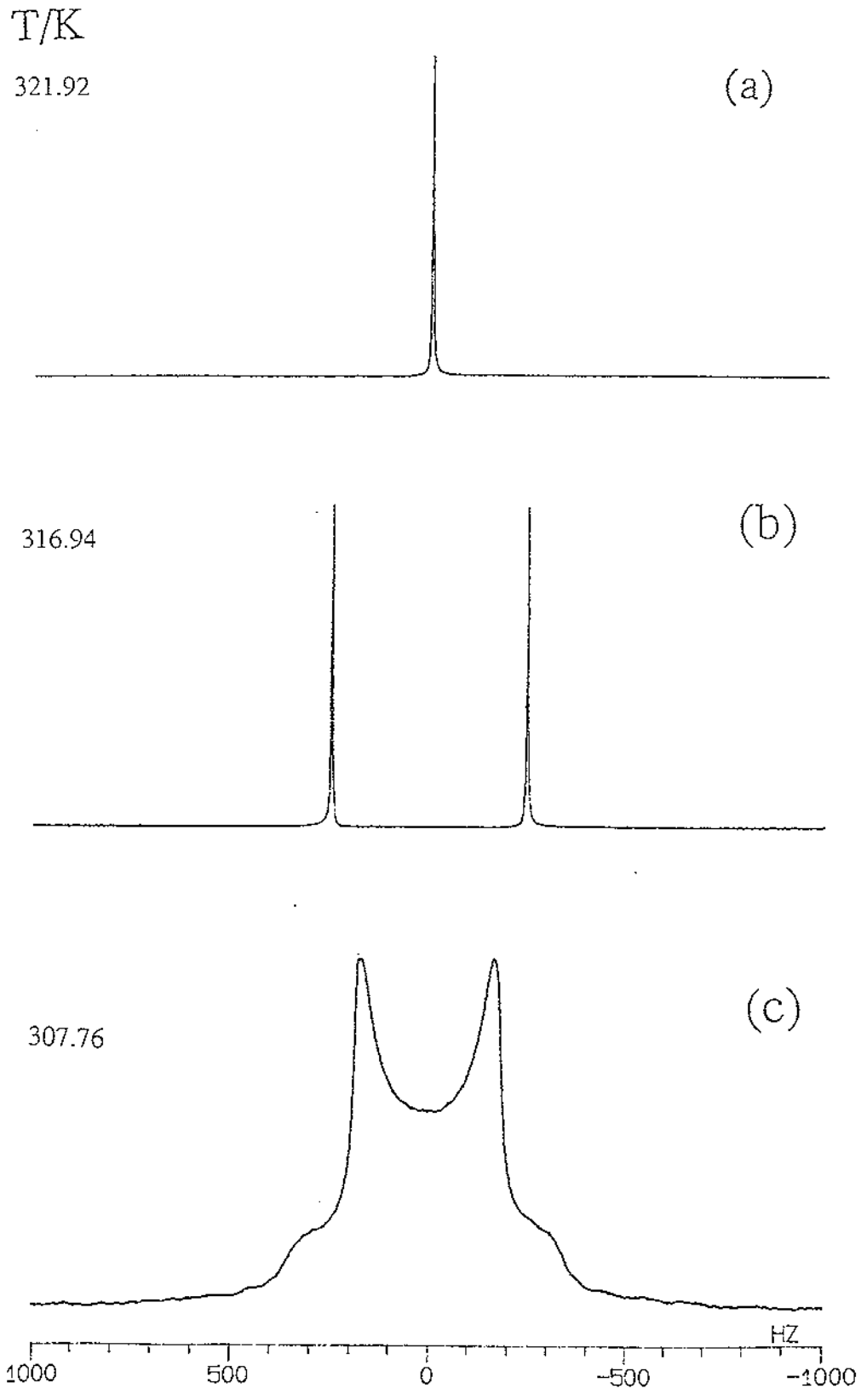

4.2.1.2 ^{133}Cs NMR spectra.

The appearance of typical ^{133}Cs spectra are shown in figure 4.2.2. As for the ^{2}H spectrum in an isotropic micellar solution the ^{133}Cs spectrum is a singlet (figure 4.2.2a).

In the nematic phase the macroscopically aligned micellar phase gives a ^{133}Cs spectrum (figure 4.2.2b) consisting of a septet with relative intensities 7:12:15:16:15:12:7 and peak separation given by equation 3.6. For a macroscopically aligned lamellar phase the ^{133}Cs spectrum is also a septet, but with quadrupole splittings greater in magnitude. The spectrum for an unoriented lamellar phase sample produced by cooling from the isotropic phase into the lamellar phase outside the spectrometer field is shown in figure 4.2.2c. Here each of the principal doublets in the spectrum of an aligned sample are replaced by a Pake powder pattern. Only the Pake singularities with separation given by $\Delta\tilde{\nu}(\phi=90°)$ in equation 3.1 are clearly visible. Upon expansion of the scale the Zeeman resonance line is seen to have a uniaxial chemical shift tensor line shape (figure 4.2.3) reflecting the uniaxial symmetry of the mesophase. The positions of $\tilde{\sigma}_{zz}(0°)$ and $\tilde{\sigma}_{zz}(90°)$ are also shown[30].

NMR spectra of mixed phases consist of the superposition of signals from individual phases, the intensities of which reflect the relative amounts of each phase present. This will be explained more fully in section 4.2.2.1.

Though it is possible to determine the phases present by examination of either ^{2}H or ^{133}Cs NMR spectra, the latter offer an order of magnitude improvement[2] over ^{2}H spectra in resolution of signals from coexisting phases and allow the observation of the anisotropy in the ^{133}Cs chemical shift as an alternative method for phase transition determination, hence ^{133}Cs spectra are largely used for this purpose.

4.2.2 Determining Phase Transition Temperatures.

The composition and temperature dependence of phase transitions in lyotropic liquid crystal systems makes it particularly important to maintain sample homogeneity. Concentration or temperature gradients along a sample lead to inhomogeneities which manifest themselves in NMR spectra as line broadening or asymmetry[32]. Thus tight temperature control is required and, to avoid the problem of phase separation, as little time as possible should be spent in mixed phase regions and every first order phase transition should be traversed from the pure phase to the mixed phase.

Generally phase transition temperatures were determined graphically by plotting the quadrupole splittings as a function of temperature. The results of a typical

Figure 4.2.2 ^{133}Cs NMR spectra for a macroscopically aligned w=0.5 CsPFO/$^{2}H_2O$ sample obtained by cooling from the isotropic (a) into the nematic phase (b). Spectrum (c) is for an unoriented lamellar phase produced by cooling the sample from the isotropic into the lamellar phase outside the magnetic field. The peaks in (c) correspond to 90° singularities and the quadrupole splitting $\Delta\tilde{\nu}$ is given by $\Delta\tilde{\nu}=\frac{1}{28}\left|\tilde{q}_{zz}\right|_S S$ compared to $\Delta\tilde{\nu} = \frac{1}{14}\left|\tilde{q}_{zz}\right|_S S$ for the 0° orientation in (b).

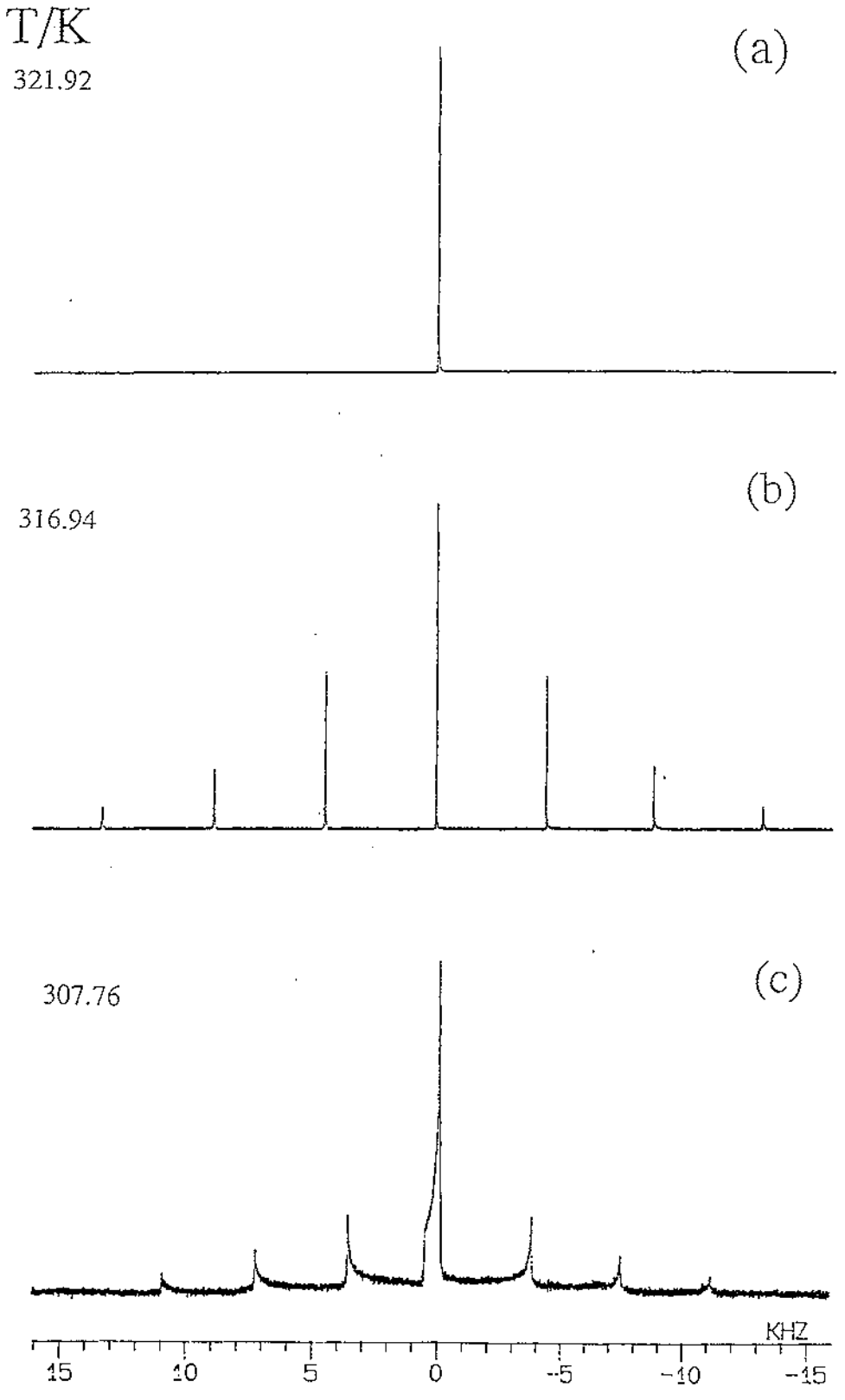

Figure 4.2.3 ^{133}Cs NMR spectrum of the Zeeman transition for an unoriented w=0.5 CsPFO/$^{2}H_2O$ sample at 307.76 K in the lamellar phase (see figure 4.2.2c) showing the location of $\tilde{\sigma}_{zz}(0°)$ and $\tilde{\sigma}_{zz}(90°)$[30]. The line shape is consistent with an isotropic distribution of director orientations and reflects the uniaxial symmetry of the mesophase.

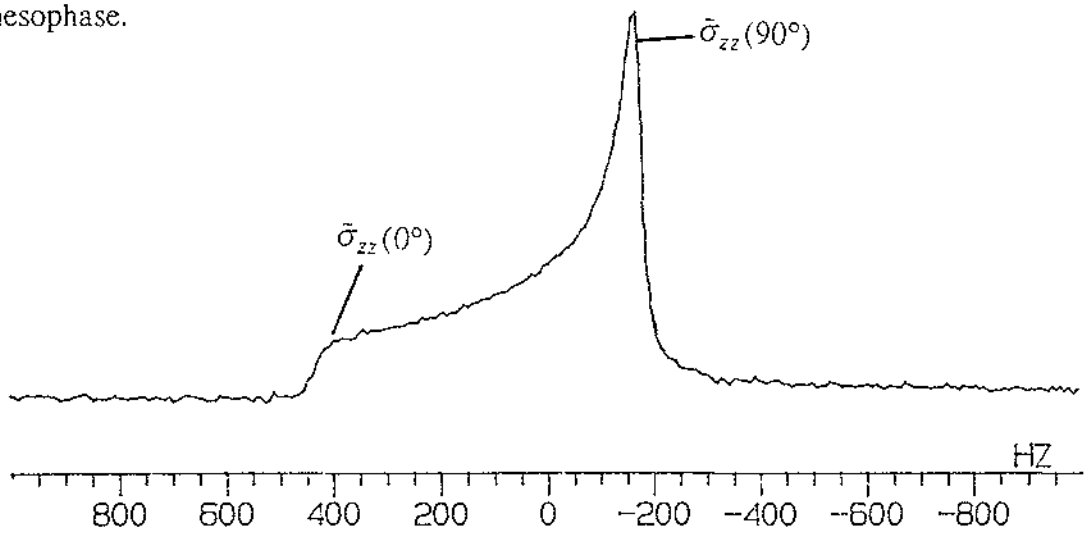

Figure 4.2.4 Temperature dependence of ^{133}Cs quadrupole splittings for a w=0.5 CsPFO/$^{2}H_2O$ sample[22].

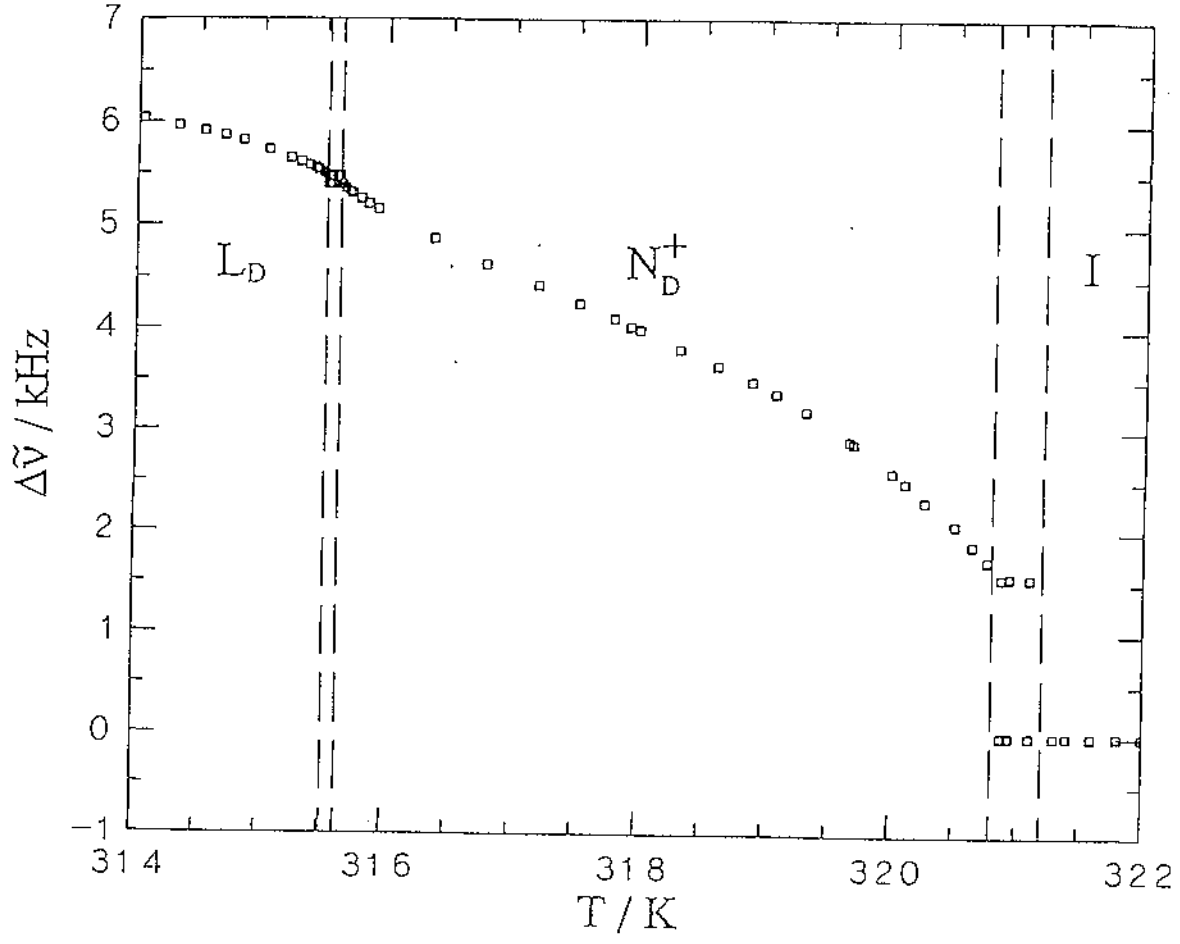

experiment are shown in figure 4.2.4 for ^{133}Cs in a pure 0.5 CsPFO/$^{2}H_2O$ sample. The changes in the magnitude of the quadrupole splittings with temperature can be related to variation of S, $\langle P_2(\cos\alpha)\rangle_S$ and β in equations 3.6 and will explored more fully in section 4.3.

The phase boundaries determined are defined below.

T_{IN} - the upper temperature limit of the isotropic/nematic biphasic region,

T_{NI} - the lower temperature limit of the isotropic/nematic biphasic region,

T_{NL} - the upper temperature limit of the nematic/lamellar biphasic region,

T_{LN} - the lower temperature limit of the nematic/lamellar biphasic region for a first order lamellar-to-nematic transition or the phase transition temperature for a second order nematic-to-lamellar transition.

The specific methods for determining phase transition temperatures will now be presented.

4.2.2.1 Determining T_{IN}.

Figure 4.2.5 shows a typical sequence of ^{133}Cs spectra observed on cooling from the isotropic towards the upper temperature boundary to the I/N_D^+ mixed phase region. The broadening of the isotropic signal (figure 4.2.5a) evident in figure 4.2.5b, and which becomes more apparent in figures 4.2.5c-d, is attributed to unresolved fine structure due to orientational ordering of the micelles induced by the magnetic field[33]. It arises from the magnetic torque acting on the micelles which is enhanced by the buildup in the angular correlations of the micelles as the transition is approached. The first appearance of this effect occurs about 80 mK above T_{IN}[33]. Generally T_{IN} was obtained by first determining a rough estimate of its value. A homogeneous isotropic sample was then cooled to within 0.5 K of T_{IN} when cooling was slowed to approximately 100 mK min^{-1} until the first appearance of the nematic Zeeman peak at about 90 Hz down field from the isotropic singlet (figure 4.2.5c). The sample temperature was then just below that of T_{IN}. After remixing the process was repeated from about 100 mK above T_{IN} cooling at approximately 20 mK min^{-1}. The temperature at which the Zeeman peak reappeared was taken as T_{IN} and by this method was accurate to within ±20 mK. A more precise method of determiningT_{IN} (to within 2 mK) is from measurements of the quadrupole splittings caused by field-induced order in the isotropic phase[33]. However, for the w=0.5 sample the field induced quadrupole splittings are too small to be used for this purpose. The first appearance of the narrow Zeeman peak of the nematic phase is much easier to detect than the broader quadrupole resonances.

Upon further cooling, the nematic phase signal in figure 4.2.5d increases in intensity and the isotropic peak diminishes in intensity, reflecting the relative amounts of each phase present, until at T_{NI} only the nematic signal remains.

T_{NI} may be obtained in a similar fashion to T_{IN} i.e. from the first appearance of the isotropic Zeeman peak on heating from the pure nematic phase. However, a much more precise technique is measuring the quadrupole splittings on heating from the pure nematic into the I/N_D^+ mixed phase region.

4.2.2.2 Determining T_{NI}.

Figure 4.2.6 shows the results of a typical experiment to determine T_{NI}. A homogeneous isotropic sample was rapidly cooled (to avoid phase separation) inside the magnet to some point midway through the nematic phase region. The sample was then slowly heated and the quadrupole splittings recorded into the isotropic/nematic biphasic region. The quadrupole splittings were plotted as a function of temperature and T_{NI} is indicated by a discontinuity in the graph. T_{NI} obtained in this way (as the intersection of two lines fitted to points above and below the transition temperature) was accurate to within ±10 mK.

4.2.2.3 Determining T_{NL} & T_{LN}.

These are also best determined from the temperature dependence of the ^2H or ^{133}Cs quadrupole splittings.

The temperature dependence of the ^2H quadrupole splittings for a w=0.4 CsPFO/^2H_2O sample is shown in figure 4.2.7. Here the nematic-to-lamellar transition is second order i.e. there is no mixed phase region and T_{LN} is indicated by a point of inflection in the graph[1]. Since $\delta\Delta\tilde{\nu}/\delta T$ for the ^2H splittings in the lamellar phase is less than that for the ^{133}Cs splittings (see section 4.3.5) the point of inflection is more pronounced in the case of the ^2H splittings.

The temperature dependence of the ^2H and ^{133}Cs quadrupole splittings for a w=0.5 CsPFO/^2H_2O sample across the nematic-to-lamellar transition is shown in figure 4.2.8. Here the transition is first order and T_{NL} and T_{LN} are indicated by a discontinuities in ^{133}Cs quadrupole splittings above and below the biphasic region respectively whereas there is no discontinuity in the quadrupole splittings of ^2H, only a discontinuity in the temperature dependence which identifies T_{LN}[1]. Figure 4.2.9 shows ^{133}Cs spectra obtained on cooling from the nematic phase through an N_D^+/L_D mixed phase into the lamellar phase. Separate signals for the N_D^+ and L_D phases are clearly observable in the mixed phase region. The corresponding ^2H spectra are shown in

figure 4.2.10 . Here the mixed phase region is barely detectable as a slight broadening in the doublet linewidths. This provides a good demonstration of the greater resolving power of the ^{133}Cs nucleus. The broadening of the ^{2}H doublet in the biphasic region (figure 4.2.10b) is a consequence of the exchange of water molecules by diffusion across the interface separating coexisting nematic and lamellar phases[1,34]. The lamellar phase nucleates as a dispersion of small droplets in a matrix of the nematic phase[1]. If the mean residence time of a water molecule or counterion in a particular phase is τ then the broadening due to this intermediate exchange regime is $1/\tau \approx 2\pi\Delta$, where $\Delta=(\Delta\tilde{\nu}_L-\Delta\tilde{\nu}_N)/2$ [1]. The increased resolution of ^{133}Cs NMR comes from the increased Δ value for this nucleus i.e ^{133}Cs can detect shorter residence times than ^{2}H.

Figure 4.2.5 Sequence of ^{133}Cs spectra[22] observed in determining T_{IN} by cooling a w=0.5 CsPFO/$^{2}H_2O$ sample from the isotropic phase, I (a and b) into the isotropic/nematic, I/N_D^+, biphasic region (c and d). Fine structure in the isotropic signal close to the transition (b) is evidence of pretransitional ordering of the micelles in the isotropic phase[33].

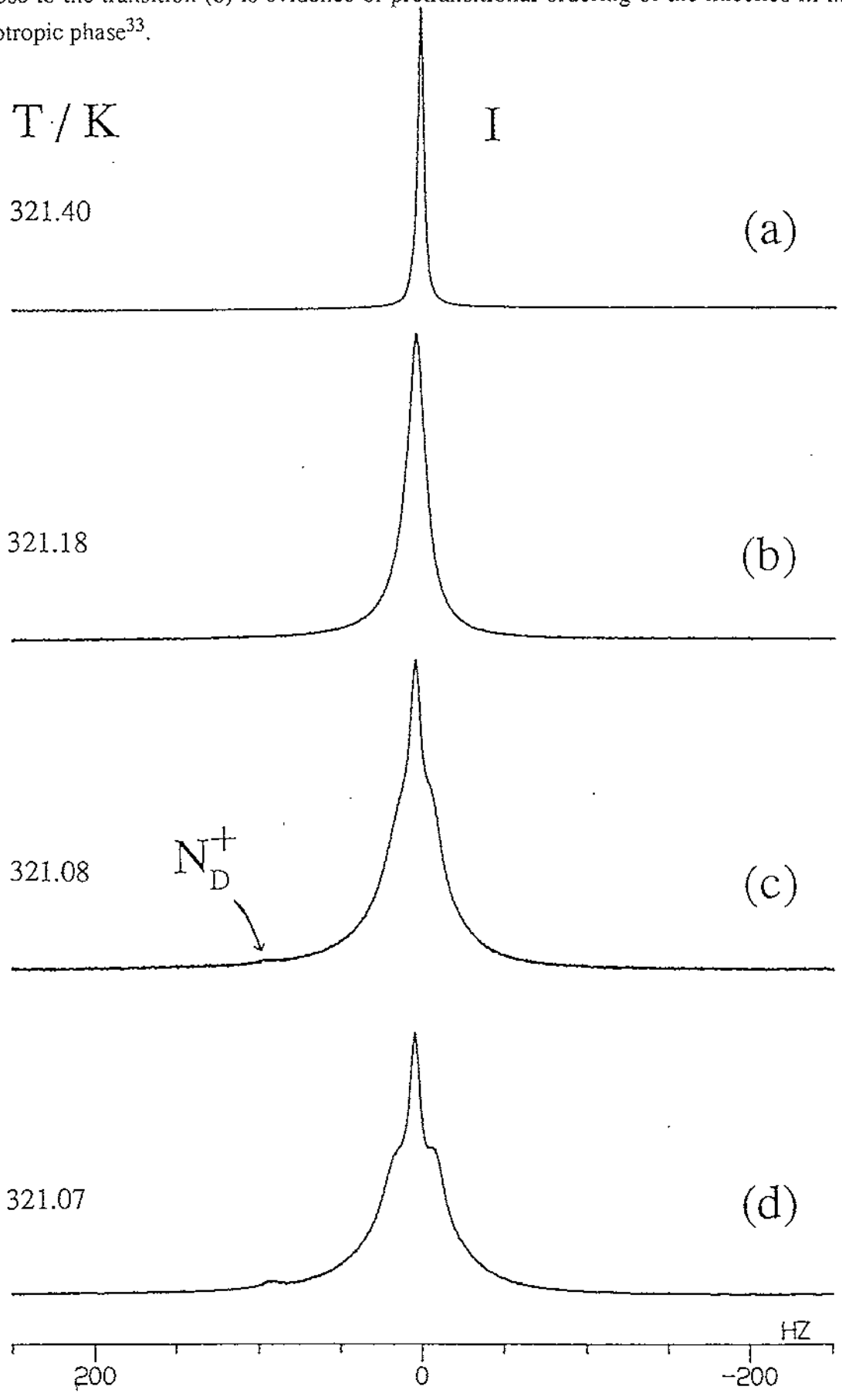

Figure 4.2.6 Temperature dependence of the ^{133}Cs quadrupole splittings $\Delta\tilde{\nu}$ for a CsPFO/D_2O/NMF sample with constant mass ratio CsPFO:D_2O of 1:1 and an NMF mole fraction of 0.00954. The discontinuity in $\Delta\tilde{\nu}$ clearly defines the location of T_{NI}.

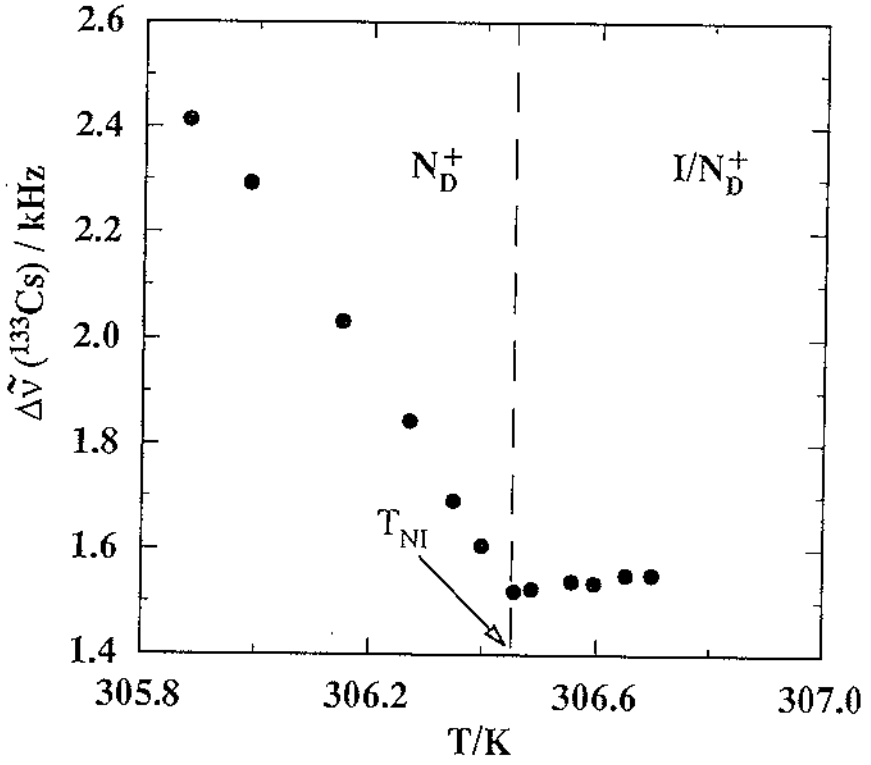

Figure 4.2.7 Temperature dependence of the ^2H quadrupole splittings $\Delta\tilde{\nu}$ for a CsPFO/^2H_2O sample with a constant mass ratio CsPFO:^2H_2O of 2:3. The point of inflection in $\Delta\tilde{\nu}$ defines the location of the second order phase transition temperature T_{LN}[1].

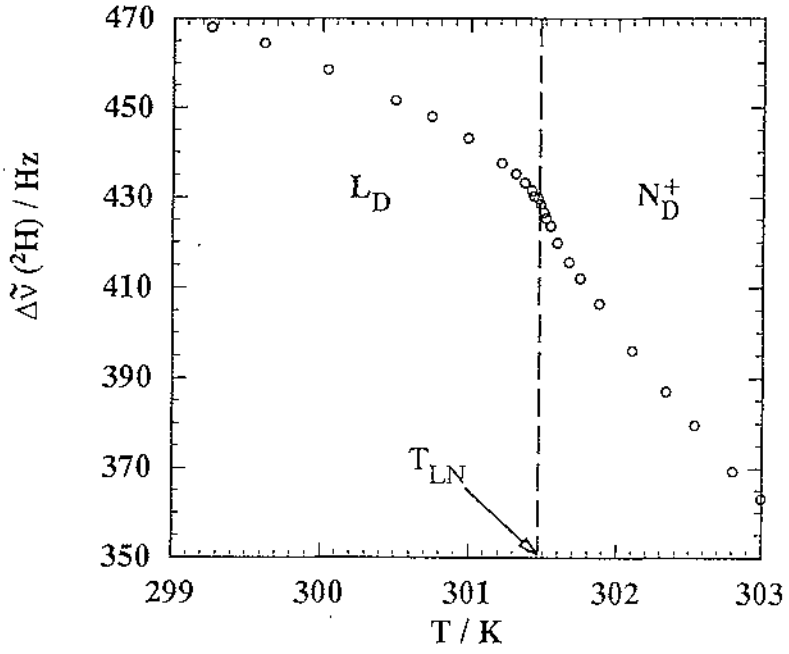

Figure 4.2.8 Temperature dependence of the ^2H and ^{133}Cs quadrupole splittings $\Delta\tilde{\nu}$ for a CsPFO/^2H_2O sample with a constant mass ratio CsPFO:^2H_2O of 1:1 and a DMF mole fraction of 0.0171. The upper (T_{NL}) and lower (T_{LN}) boundaries to this first order phase transition are clearly located by discontinuities in the ^{133}Cs quadrupole splittings whereas only T_{LN} can be located by ^2H quadrupole splittings. This figure and the sequence of spectra in figures 4.2.9 and 4.2.10 clearly show the greater resolving power of ^{133}Cs spectra over those of ^2H.

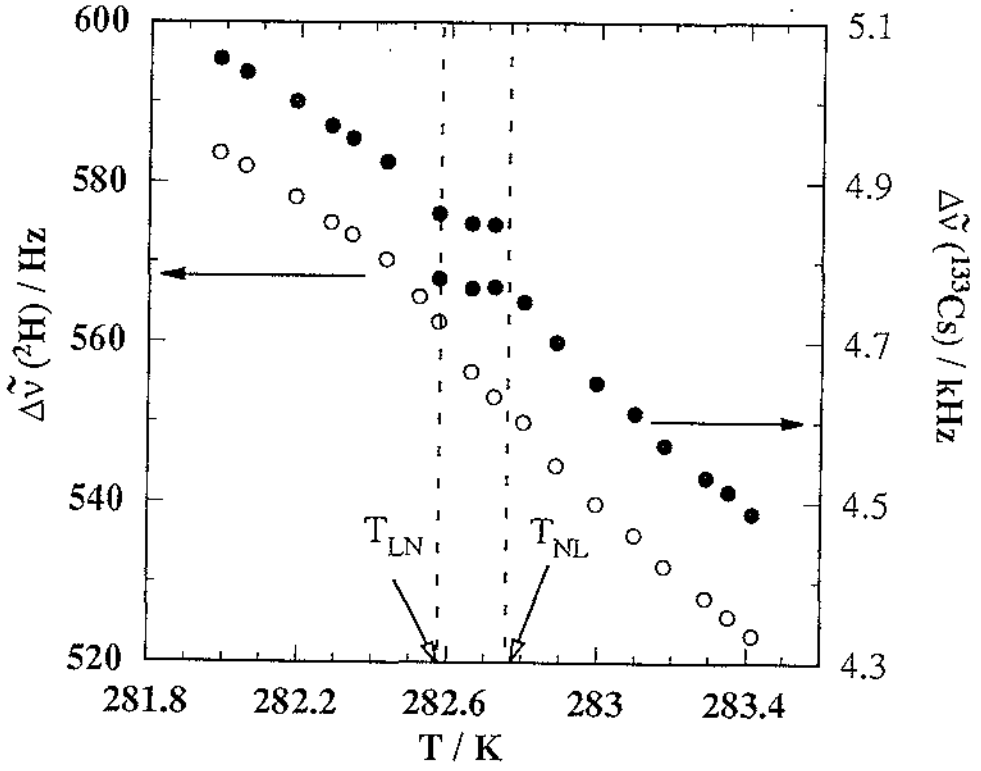

Figure 4.2.9 Sequence of ^{133}Cs NMR spectra observed upon cooling a sample with a constant CsPFO:$^{2}H_2O$ mass ratio of 1:1 and a DMF mole fraction of 0.0171 from the nematic phase (a) through an N_D^+/L_D biphasic region (b) to the lamellar phase (c). Separate signals from both phases are clearly resolved in (b).

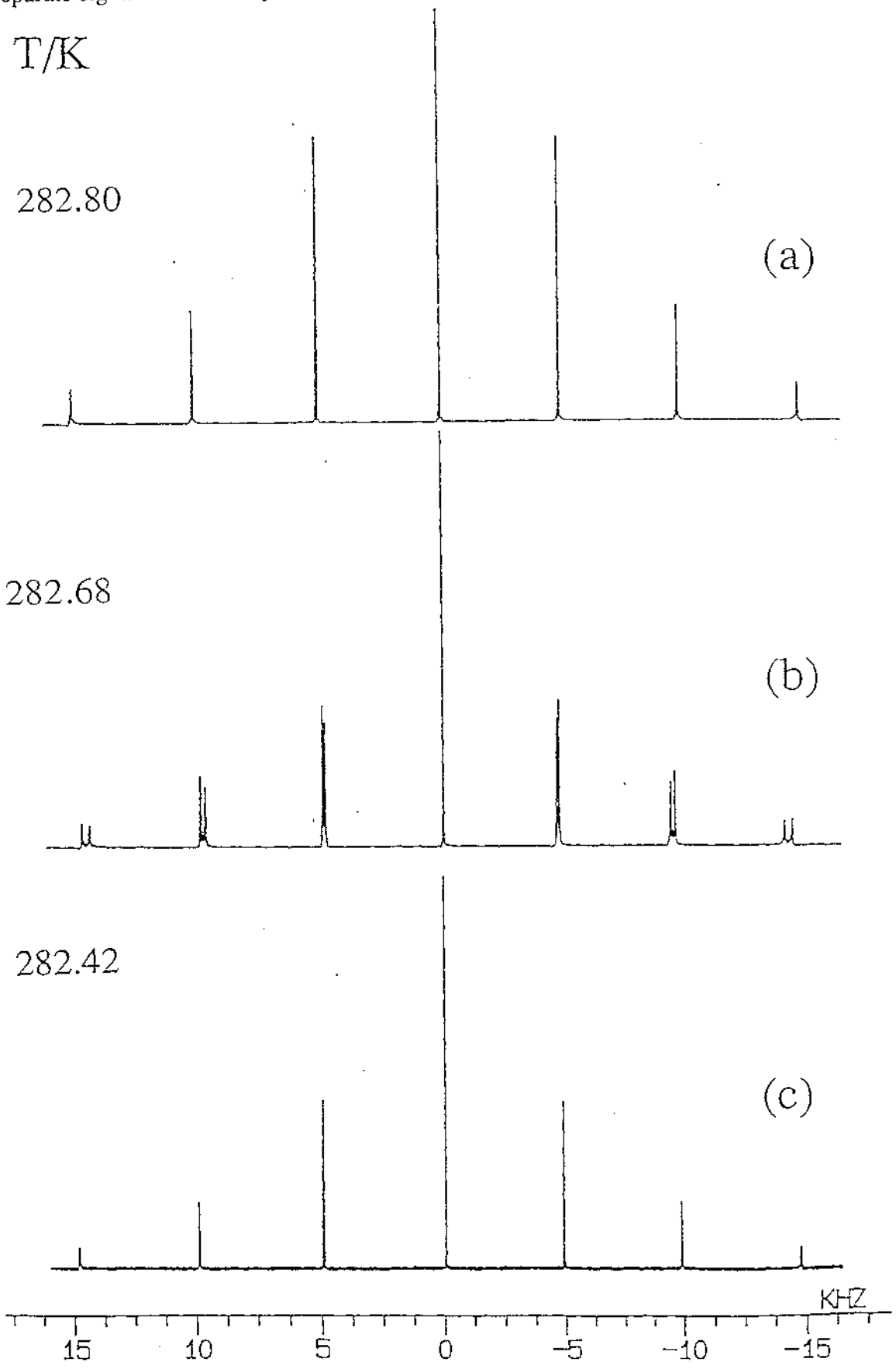

Figure 4.2.10 Sequence of ^{2}H NMR spectra observed upon cooling a sample with constant CsPFO:$^{2}H_2O$ mass ratio of 1:1 and a DMF mole fraction of 0.0171 from the nematic phase (a) through an N_D^+/L_D biphasic region (b) to the lamellar phase (c). Evidence of the presence of a mixed phase is merely a slight broadening of the doublet line shape (cf figure 4.2.9). This is a clear example of the greater resolving power of ^{133}Cs spectra with respect to ^{2}H spectra.

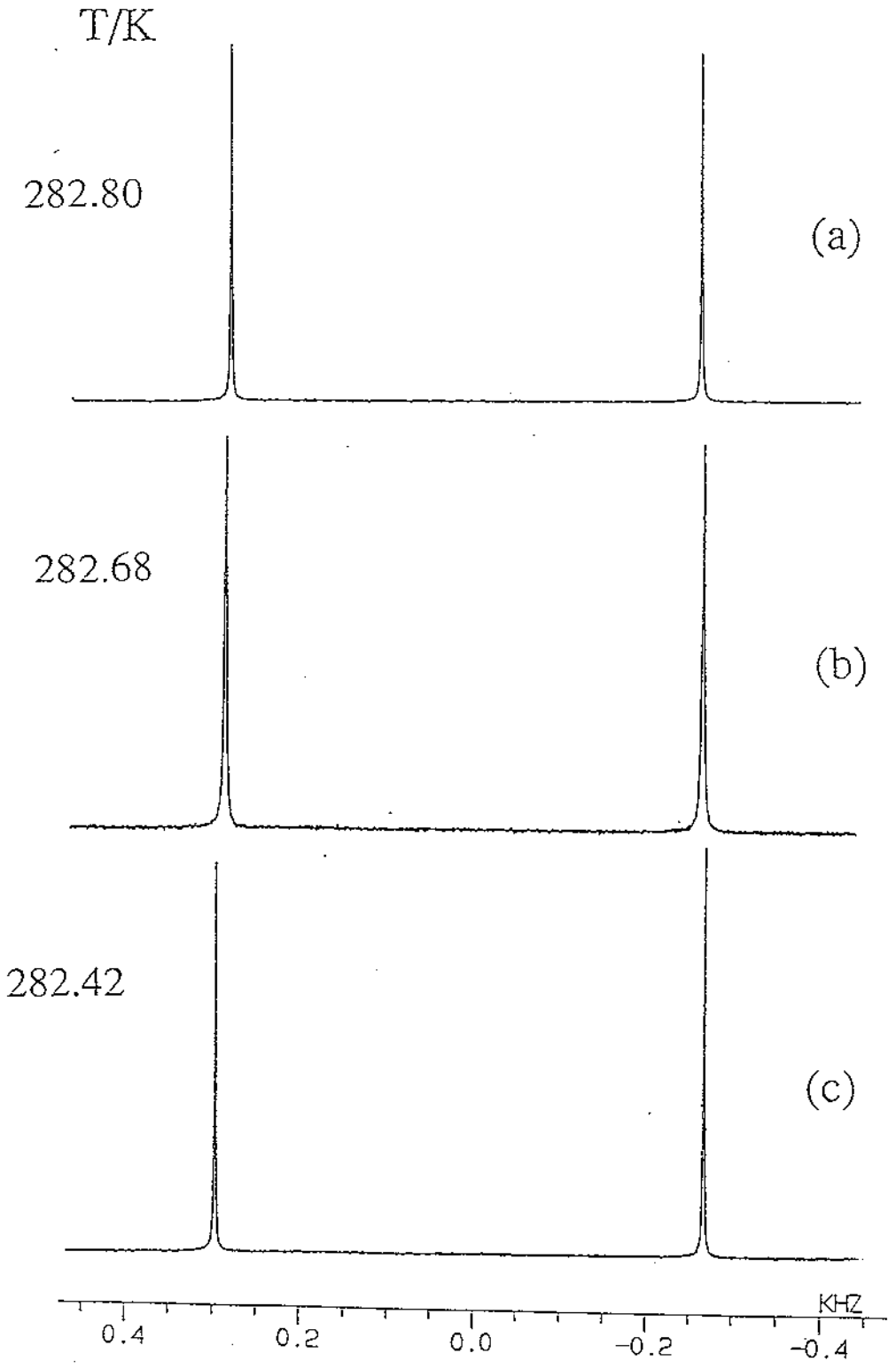

4.3 The Effect of Co-solvent on Micelle Size.

4.3.1 Introduction

Within the framework of a hard particle model (see introduction), the micelle should have the same axial ratios (*a/b*) at corresponding volume fractions irrespective of the solvent system. In the binary CsPFO/D_2O system, small angle x-ray scattering experiments[5] have established the temperature/composition dependence of micelle size. At any given temperature the micelle aggregation number initially increases with concentration, reaching a maximum at a weight fraction of CsPFO of about 0.45, and then decreases as the concentration is further increased, whilst at any given concentration the aggregation number decreases monotonically with increasing temperature. Along the nematic-to-isotropic transition line at T_{NI} and the lamellar-to-nematic transition line at T_{LN} the micelles decrease in size with increasing volume fraction ϕ of surfactant as would be expected from a hard particle interaction. There is a parallel relationship between *a/b* and ϕ along the T_{LN} and T_{NI} transition lines with a small displacement of *a/b* to smaller values at T_{LN} . The axial ratios at a ϕ of 0.321 (w=0.5) are 0.28 atT_{LN} and 0.32 atT_{NI}. The value at T_{NI} is predicted to be 0.28 by the Taylor/Hertzfeld[18] which is pleasingly close to the observed 0.32. There is, however, poor aggreement between the model and the value at T_{LN}. In the model the predicted a/b vs ϕ relationship is displaced to lower a/b and higher ϕ values, and at a ϕ of 0.32 there is no corresponding value for a/b. The difference probably arises from the model's somewhat crude cell description of the smectic (lamellar) phase[18,35]. Further x-ray studies would be required to determine the specific ϕ dependence of the *a/b* ratios in the co-solvent systems but a comparison of the micelle sizes between the four systems can be obtained from the magnitudes of the ^2H quadrupole splittings of heavy water in the four systems.

The quantity $\langle P_2(\cos\alpha)\rangle_s = \langle \frac{3}{2}\cos^2\alpha - \frac{1}{2}\rangle_s$ in equation 3.4 can be calculated from the axial ratio a/b of the micelles[1]. Furthermore, it has been established from studies on the CsPFO/D_2O[1] and APFO/D_2O[3] systems that over the temperature and concentration ranges of the nematic phases the product $\chi_D n_b S_{OD}$ is constant so that for a given sample concentration the variation in the quadrupole splittings can be explained solely in terms of changes in S and $\langle P_2(\cos\alpha)\rangle_s$. It has been shown[2,3] that the variation in quadrupole splittings is precisely reproduced, in both the APFO/D_2O and CsPFO/D_2O systems, by the changes in the quantity $S\langle P_2(\cos\alpha)\rangle_S$. Thus, changes in $S\langle P_2(\cos\alpha)\rangle_s$ over a concentration/temperature range can be monitored by calculating the quantity $\Delta\tilde{\nu}/(x_A/x_W)$. For all the samples considered in this study the ratio x_A/x_W is constant (= 0.0366) and so the variation in micelle size may be monitored by simply

measuring the value of the ^2H quadrupole splittings $\Delta\tilde{\nu}$. Of course the volume fraction of surfactant decreases with the amount of added co-solvent which may lead to a corresponding decrease in the a/b ratio at the transition temperature[5]. The magnitude of the effect is small however and at the maximum co-solvent concentration used here only a 2% decrease in a/b is expected. For the purposes of this study these possible small changes can be ignored.

4.3.2 Variation of Micelle Size with Temperature.

Figure 4.3.1 shows a typical plot of the temperature dependence of $\Delta\tilde{\nu}(^2H)$. Through the biphasic I/N_D^+ region the quadrupole splittings of the nematic phase are roughly constant as a consequence of a constant S at T_{NI}. On cooling below T_{NI}, the quadrupole splittings show a rapid increase which eases off before increasing again as T_{NL} is approached. This increase is mainly reflecting the increase in S on cooling through the nematic phase. The increase in quadrupole splittings with decreasing temperature below T_{LN} is mainly due to an increasing $\langle P_2(\cos\alpha)\rangle_S$ since S is known to increase only slowly in the lamellar phase. An increase in $\langle P_2(\cos\alpha)\rangle_S$ is a consequence of a decrease in the a/b ratio, i.e. the micelle size increases with decreasing temperature. This conclusion is supported by x-ray evidence[5].

4.3.3 Variation of Micelle Size with Co-solvent.

Figure 4.3.2 shows the ^2H quadrupole splittings along the 290.87 K isotherm in the lamellar phase as a function of mole fraction DMF added to samples with a constant CsPFO to D_2O mass ratio of 2:3. Figure 4.3.3 shows the same for samples with a constant CsPFO to D_2O mass ratio of 1:1 along the 279.07 K isotherm. It is clear that $\Delta\tilde{\nu}(^2H)$ decreases with added co-solvent and the decrease is more for DMF than FA at corresponding mole fractions. The decrease in $\Delta\tilde{\nu}(^2H)$ can only arise from a corresponding decrease in $\langle P_2(\cos\alpha)\rangle_S$ since the orientational order parameter varies only slightly in the lamellar phase[4]. Thus the effect of co-solvent is to produce smaller micelles (higher a/b ratio).

4.3.4 Variation of Micelle Size along the Phase Transition Lines.

Figure 4.3.4 shows the ^2H quadrupole splittings at the phase transition temperatures T_{NI} and T_{LN}. It is clear from this figure that $\Delta\tilde{\nu}(^2H)$ is essentially constant along both transition lines. The widths of the N_D^+/I and N_D^+/L mixed phase regions and the temperature range of the nematic phase are unaffected by the amount of co-solvent added which implies that the strengths of the I-to-N_D^+ and N_D^+-to-L_D transitions remain the same. We may therefore expect the values of S at the transitions to be constant[3]. A constant value for $\Delta\tilde{\nu}$ therefore implies constant micelle size along the transition lines.

4.3.5 Micelle Size and Bound-ion Fraction β.

From examination of equations 3.6 and 3.9 for the quadrupole splittings and the chemical shift anisotropy of the ^{133}Cs nucleus it is clear that in addition to the quantities S and $\langle P_2(\cos\alpha)\rangle_S$ these are determined by the value of the Cs^+ bound-ion fraction β. Furthermore, it is easily shown that chamges in the ^{133}Cs quadrupole splittings and chemical shift anisotropies have a common origin by plotting the reduced quantities

$$\frac{\Delta\tilde{\nu}_T}{\Delta\tilde{\nu}_{T_{NI}}} = \frac{\left(\beta\langle P_2\cos\alpha\rangle_S S\chi\right)_T}{\left(\beta\langle P_2\cos\alpha\rangle_S S\chi\right)_{T_{NI}}}$$

and

$$\frac{\Delta\tilde{\sigma}_T}{\Delta\tilde{\sigma}_{T_{NI}}} = \frac{\left(\beta\langle P_2\cos\alpha\rangle_S S(\sigma_\parallel-\sigma_\perp)_M\right)_T}{\left(\beta\langle P_2\cos\alpha\rangle_S S(\sigma_\parallel-\sigma_\perp)_M\right)_{T_{NI}}}$$

against each other as shown in figure 4.3.5. Differences in these quantities can only arise from differences in the temperature dependence of χ and $(\sigma_\parallel-\sigma_\perp)_M$. The fact that they are equal to each other over the full temperature range means that either they are both temperature independent or they have identical dependencies. It has been shown that in lyotropic liquid crystals which consist of "classical lamellar bilayers", in which neither the lamellar structure or the order parameter vary with temperature, that the observed quadrupole splittings of counterions are temperature independent[29,36]. It is, therefore, likely that both χ and $(\sigma_\parallel-\sigma_\perp)_M$ are temperature independent and

changes in $\Delta\tilde{\nu}(^{133}Cs)$ reflect changes in $S\langle P_2(\cos\alpha)\rangle_s\beta$. Figure 4.3.6 compares the temperature dependence of ^2H and ^{133}Cs quadrupole splittings and the ^{133}Cs chemical shift anisotropies. From the observation that $\Delta\tilde{\nu}_r(^{133}Cs)$ and $\Delta\tilde{\sigma}_r(^{133}Cs)$ are greater than $\Delta\tilde{\nu}_r(^2H)$ at any given temperature it is clear that an additional contribution is present in the case of the ^{133}Cs parameters. This must be an increase in β as the micelle size increases[2]. A corresponding increase was observed in the bound fraction of ammonium ions in the related APFO/D_2O system[3]. In both cases the increase was attributed to a preference of the counter-ions for sites with the smaller radius of curvature (higher charge density).

The isotropic ^{133}Cs chemical shifts σ_i (equation 3.10) were measured at 320.01 K as a function of co-solvent concentration and the results are presented in figure 4.3.7. For the binary system there is a shift to high field as the surfactant concentration increases at constant temperature which is consistent with an increased fraction of bound ions β and a bound ion shift to higher field of that of the free ion ($\sigma^b>\sigma^f$) (equation 3.10)[2]. In the ternary system the shift to lower fields on increasing the co-solvent concentration is probably caused by change in β. A shift to low fields will be brought about by a decrease in β.

4.3.6 Summary.

By measuring the ^2H quadrupole splittings it has been shown that the micelles sizes are a sensitive function of temperature and the amount of co-solvent present. As co-solvent is added the micelle size decreases. As the temperature is lowered micelle size increases. However, along the transition lines there is no variation in micelle size, a result which supports a hard particle interaction as being the driving force for the transition both at the isotropic-to-nematic and the nematic-to-lamellar transitions The influence of co-solvent on the aggregation process in dilute surfactant solutions will be considered in the following chapter .

Figure 4.3.1 A typical plot of the temperature dependence of the deuterium quadrupole splittings $\Delta\tilde{\nu}(^2H)$. The sample has a constant ratio of CsPFO to D_2O at 2:3. The form of the graph can be related to variation of parameters in equation 3.4.

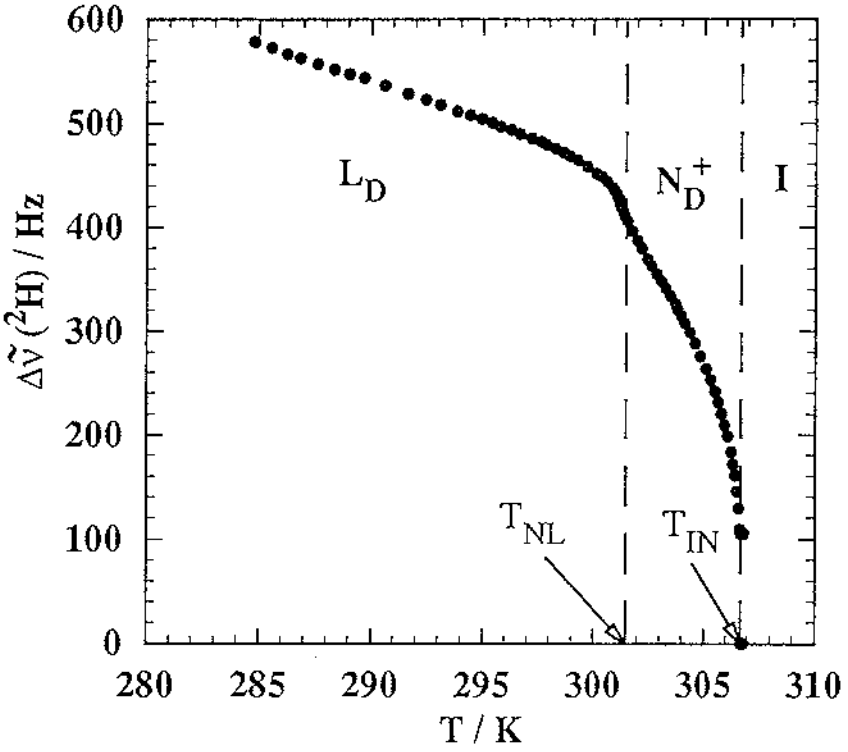

Figure 4.3.2 Deuterium quadrupole splittings $\Delta\tilde{\nu}(^2H)$ along an isotherm in the lamellar phase at 290.87 K as a function of added DMF in samples with a constant mass CsPFO to D_2O mass ratio of 2:3.

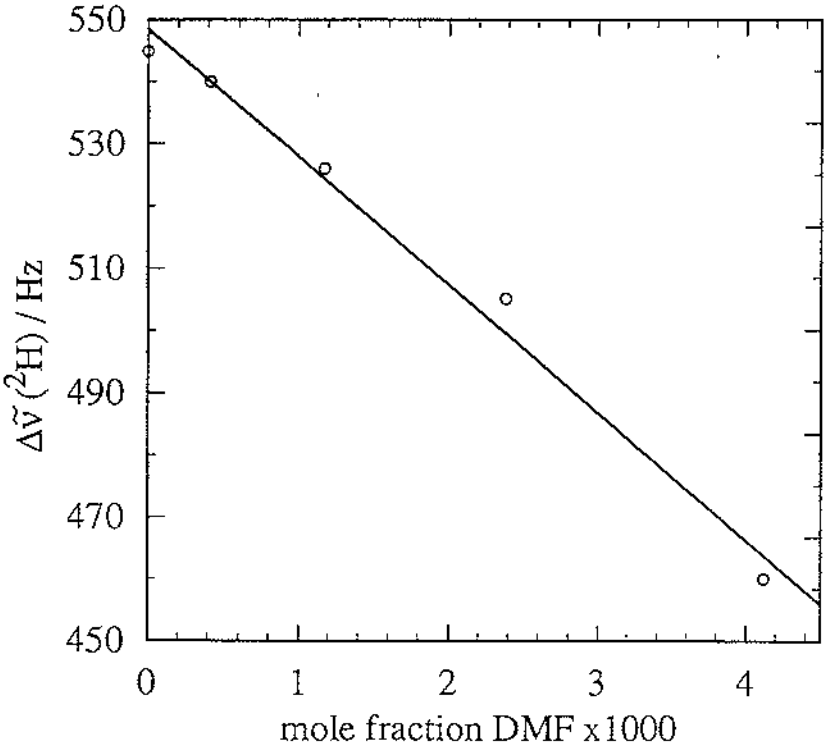

Figure 4.3.3 Deuterium quadrupole splittings $\Delta\tilde{\nu}(^2H)$ along an isotherm in the lamellar phase at 279.07 K as a function of added FA and DMF in samples with a constant CsPFO to D_2O mass ratio of 1:1.

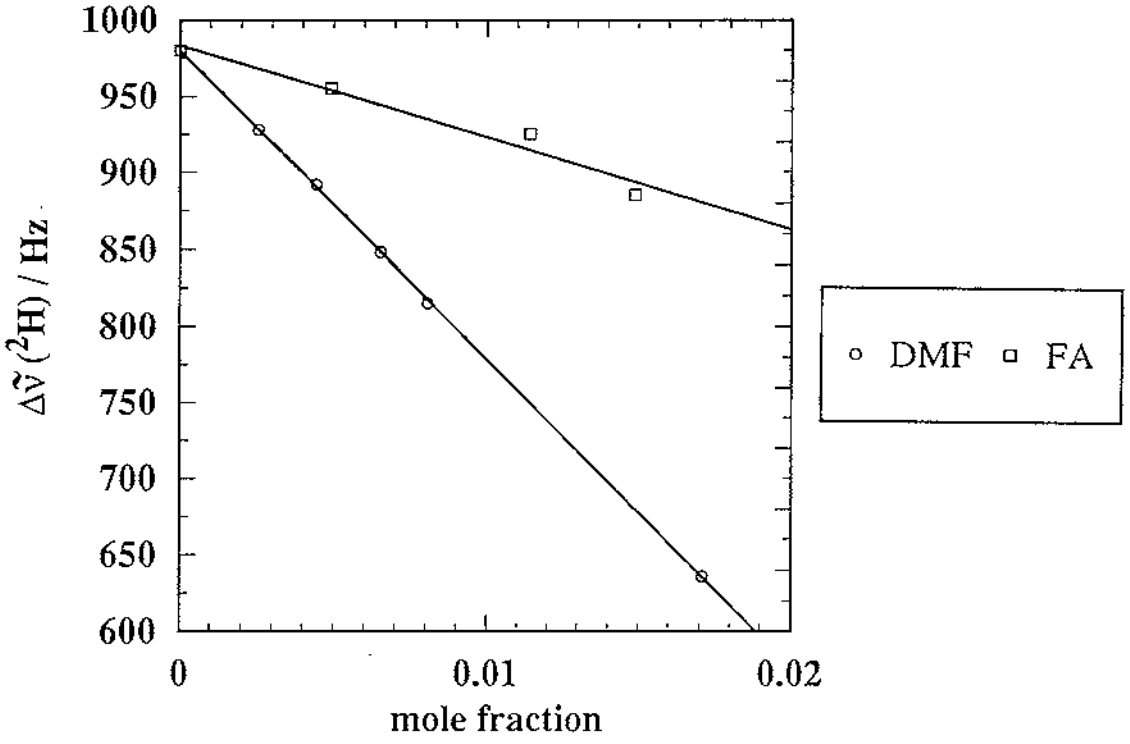

Figure 4.3.4 Deuterium quadrupole splittings $\Delta\tilde{\nu}(^2H)$ at the phase transition temperatures T_{IN} and T_{LN} as a function of added co-solvent in samples with a constant CsPFO to D_2O mass ratio of 1:1.

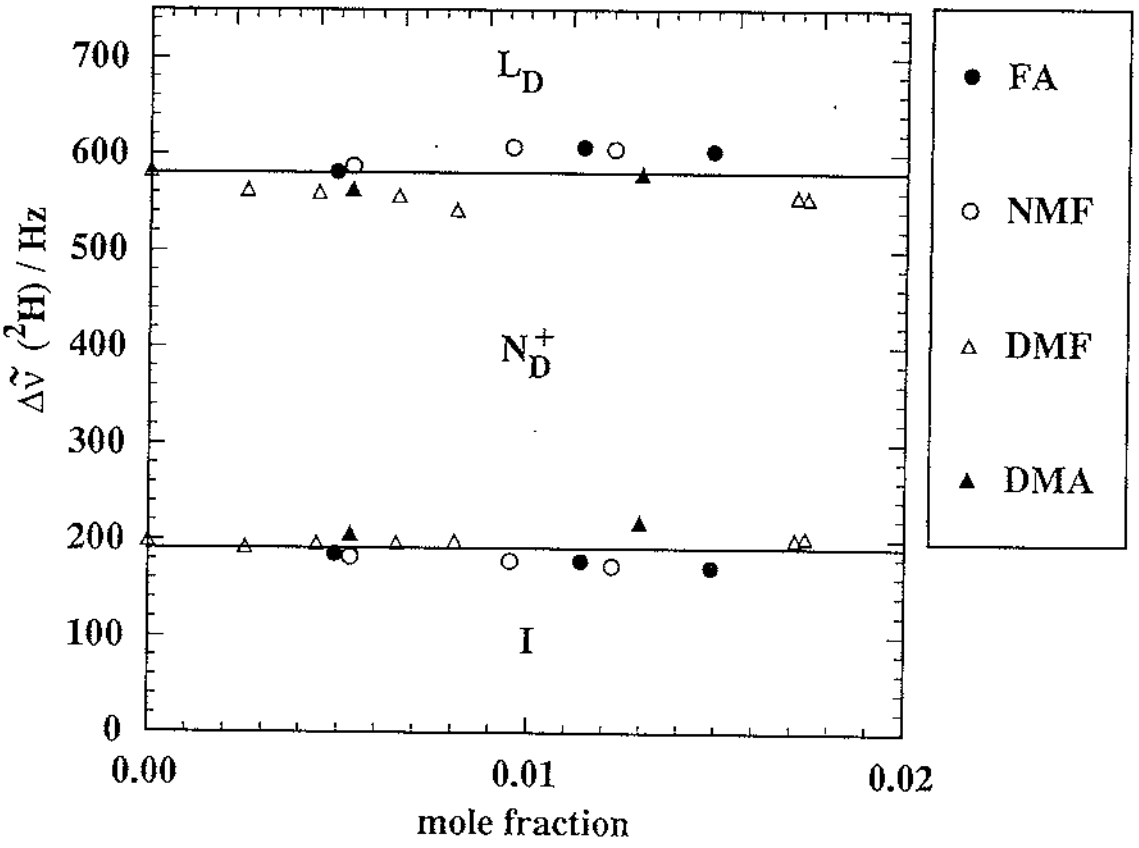

Figure 4.3.5 The plot of reduced caesium quadrupole splittings $\Delta\tilde{\nu}_r(^{133}Cs)$ vs reduced caesium chemical shift anisotropies $\Delta\sigma_r(^{133}Cs)$ (see section 4.3.5 for a definition of reduced quantities) in a w=0.5 CsPFO/D_2O sample[22].

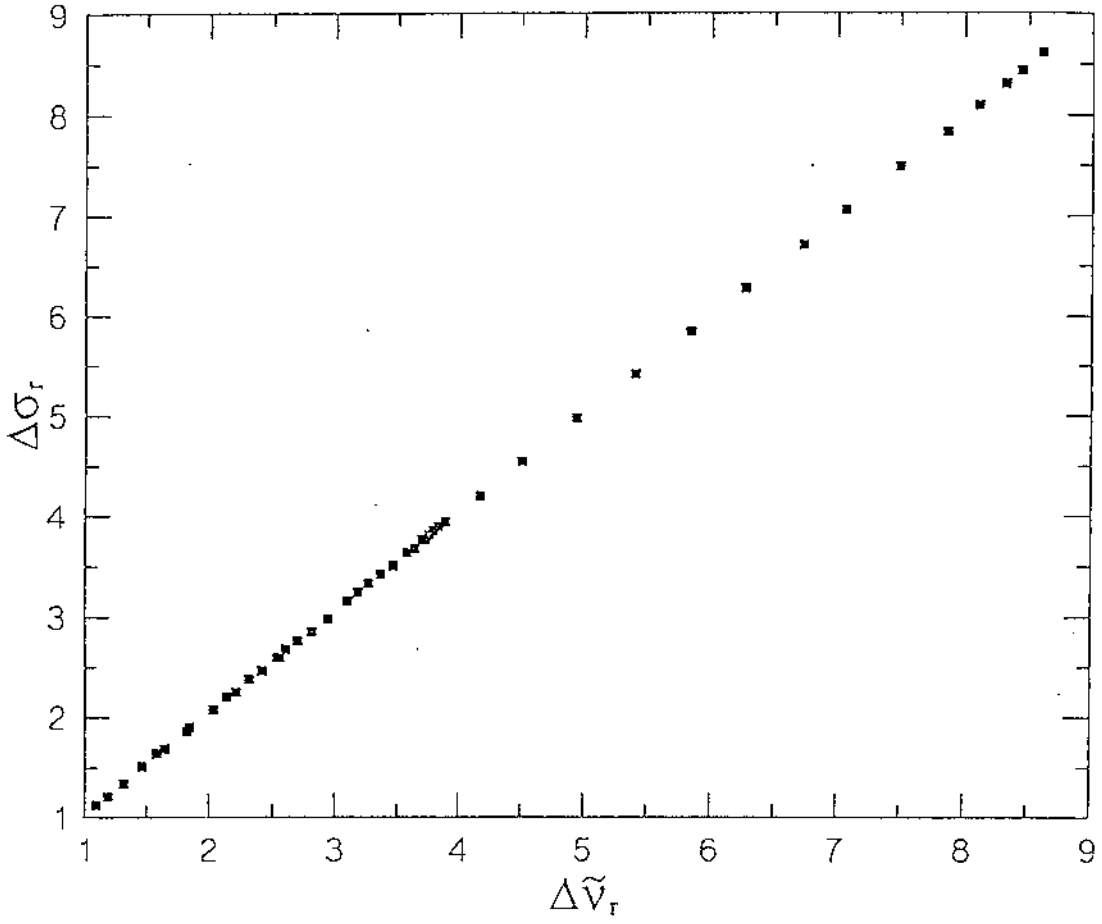

Figure 4.3.6 The temperature dependence of the reduced ^{2}H quadrupole splittings and reduced ^{133}Cs quadrupole splittings and chemical shift anisotropies (see section 4.3.5 for a definition of reduced quantities) in a sample with a constant CsPFO to D_2O mass ratio of 1:1 and DMA mole fraction of 0.0123.

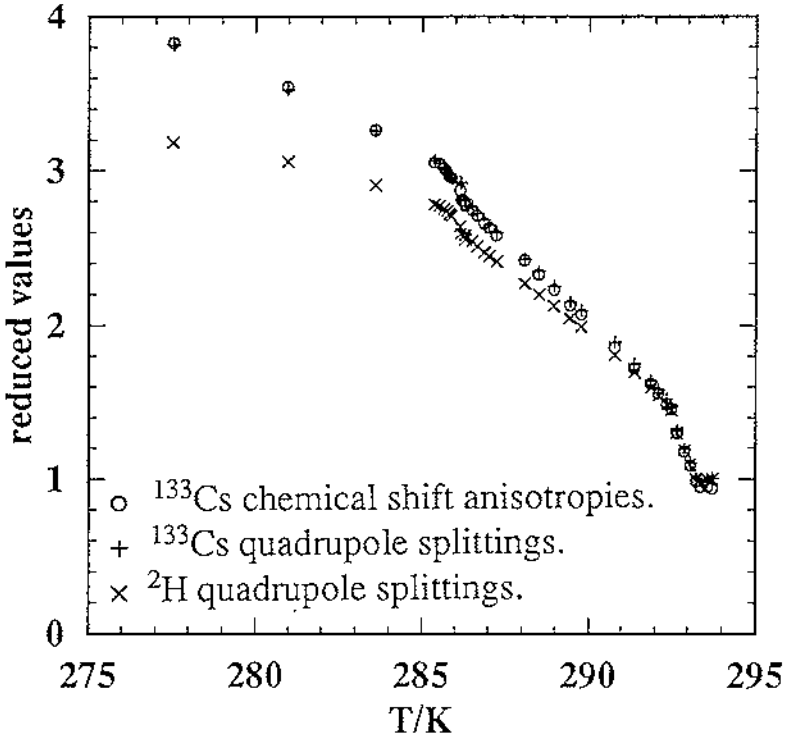

Figure 4.3.7 The isotropic ^{133}Cs chemical shifts σ_i at 320.01 K as a function of co-solvent concentration in samples with a constant CsPFO:D_2O mass ratio of 1:1 (referenced to the ^{133}Cs chemical shift at infinite dilution in D_2O). Positive shifts are to high field of the reference.

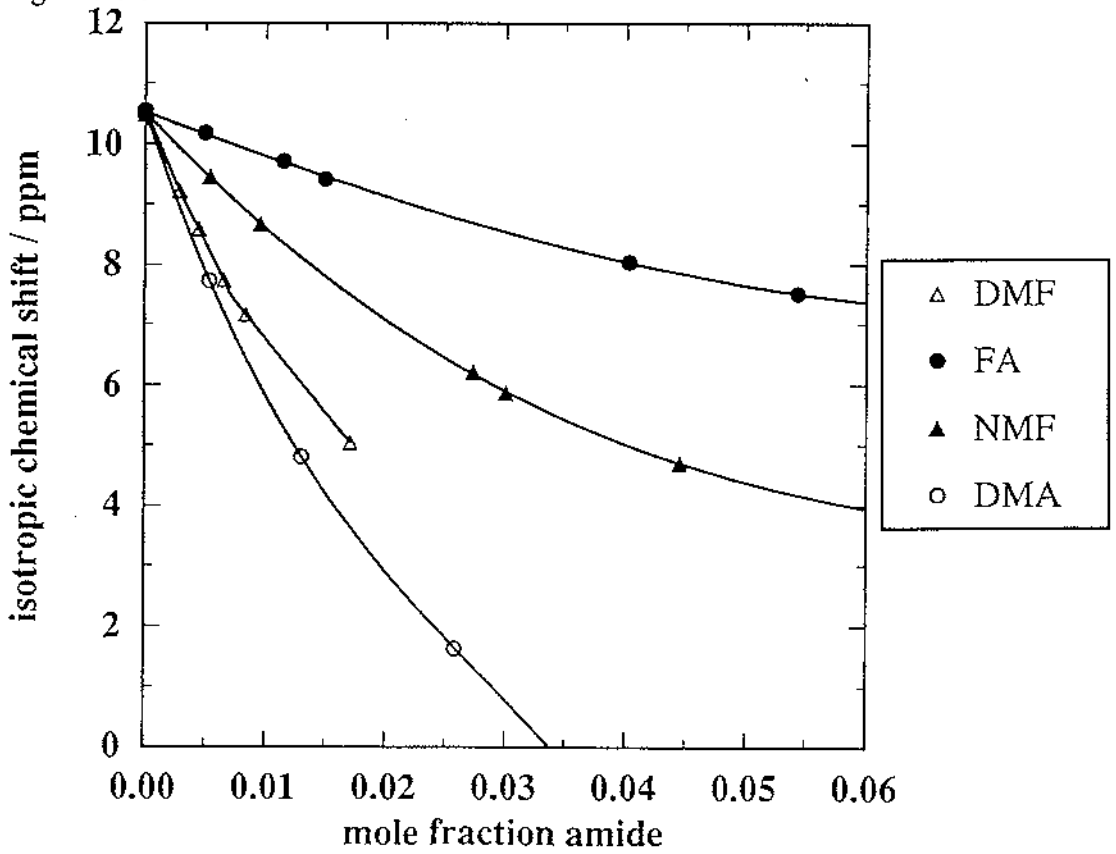

5.The Effect of Cosolvent on Self-Assembly in dilute CsPFO/D_2O Solutions.

5.1. Self-Assembly.

The process of self-assembly of molecules of nonionic surfactant S may be considered to be an equilibrium between monomers in solution and molecules in a micelle with aggregation number N thus

$$N\mathbf{S} \underset{k_1}{\overset{k_N}{\rightleftharpoons}} \mathbf{S_N} \ .$$

From the law of mass action the following may be written :

$$\text{the rate of association} = k_1 X_1^N \qquad 5.1$$

$$\text{the rate of dissociation} = k_N(X_N/N) \qquad 5.2$$

where X_N is the concentration of molecules in an *N*-mer. Assuming ideal mixing the equilibrium constant for the above process may be expressed as

$$K = \frac{k_1}{k_N} = \exp\left[\frac{-N(\mu_N^0 - \mu_1^0)}{kT}\right] \qquad 5.3$$

where μ_N^0 is the mean interaction free energy per molecule in an *N*-mer and μ_1^0 is the mean interaction free energy per monomer in solution which will be used as an arbitrary reference state. Equations 5.1-3 combine to give an expression for the concentration of molecules in an *N*-mer as a function of the aggregation number and the difference in chemical potential of molecules in a disperse (monomer) and aggregated state:

$$X_N = N\left\{X_1 \exp\left[\frac{\left(\mu_1^0 - \mu_N^0\right)}{kT}\right]\right\}^N \ . \qquad 5.4$$

The total solute concentration C is given by

$$C = \sum_{N=1}^{\infty} X_N \qquad 5.5$$

and it should be noted that neither C nor X_N can exceed unity. Equations 5.4 and 5.5 are fundamental equations of self-assembly.

The necessary condition for the formation of large stable aggregates i.e. for appreciable X_N, is that $\mu_N^0 < \mu_1^0$ for some value of N, for example, when μ_N^0 progressively decreases as N increases or when μ_N^0 has a minimum value at some finite value of N. The dependence of μ_N^0 on N is usually determined by the geometrical shape of the aggregate and, since equation 5.4 is a distribution function, the exact functional variation of μ_N^0 with N determines the aggregates' mean size and polydispersity. Spheres will only be considered here since this is the probable geometry that N PFO^- amphiphiles will adopt upon aggregating[37].

If αkT is the monomer-monomer 'bond' energy in the aggregate relative to isolated monomers in solution then an expression for the chemical potential of a molecule in a spherical aggregate is[38]

$$\mu_N^0 = \mu_\infty^0 + \alpha kT / N^{1/3} \qquad 5.6$$

where μ_∞^0 is the 'bulk' energy of a molecule in an infinite aggregate. Equation 5.6 satisfies the condition for aggregate formation i.e. μ_N^0 decreases progressively with N.

The concentration at which aggregates form i.e. the CMC, can be obtained by incorporating equation 5.6 into equation 5.4. I.e.

$$X_N = N\left\{X_1 \exp\left[\alpha(1-1/N^{1/3})\right]\right\}^N \approx N\left[X_1 e^{\alpha}\right]^N \qquad 5.7$$

At low monomer concentrations X_1 such that $X_1 e^{\alpha} << 1$ it follows that $X_1 > X_2 > X_3 > \ldots$ for all α. Thus at low concentrations most molecules will be isolated monomers i.e., $X_1 \approx C$ which is shown figure 5.1.

Since X_N can never exceed unity it is clear from equation 5.7 that X_1 cannot exceed $e^{-\alpha}$. The monomer concentration $(X_1)_{crit}$ at which this occurs is the *critical micelle concentration* (CMC). Increasing the amphiphile concentration results in the formation of more aggregates while leaving the monomer concentration more or less

unchanged at the CMC value which is also shown in figure 5.1. Thus the CMC can be defined by the equation

$$\left(X_1\right)_{crit} = CMC \approx \exp\left[-\left(\frac{\mu_1^0 - \mu_N^0}{kT}\right)\right] \approx e^{-\alpha} \qquad 5.8$$

In the system under study here the self-assembly may be expressed

$$_N\mathrm{PFO}^- + {}_pCs^+ \rightleftarrows \mathrm{PFO}_N Cs_p^{z-}$$

where z is the charge on the micelle, and $p = N - z$ is the number of counterions associated with the micelle. It is now convenient to refer to free energy change on a molar basis (ΔG) rather than on a molecular basis ($\Delta\mu$). The free energy of micellisation per mole of monomer can be expressed as[2]

$$\Delta G^\circ = -RT\left\{\frac{\ln[PFO_NCs_p{}^{z-}]}{N} - \ln[PFO^-] - \beta\ln[Cs^+]\right\}, \qquad 5.9$$

where $\beta = p/N$ is the fraction of bound Cs^+ ions. For large N, the first term in brackets in equation 5.9 is often ignored and in the absence of knowledge of N in mixed amide/D_2O solvents it will also be ignored here. It has been shown[2] that in the CsPFO/D_2O system this approximation will lead to a small error of up to 3% in ΔG°, depending on the value for β. A further approximation is that, at the CMC, $[PFO^-] \approx [Cs^+] \approx CMC$. Applying these approximations to equation 5.9 allows a much simplified expression for ΔG°, i.e.

$$\Delta G^\circ \approx RT(1+\beta)\ln CMC. \qquad 5.10$$

Figure 5.1 A schematic representation of monomer and aggregate concentrations as a function of total concentration.(From Israelachvili[38])

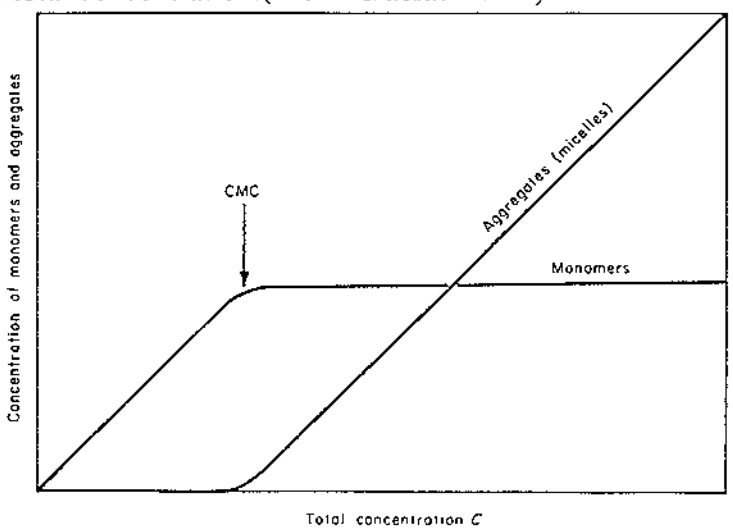

5.2. Measurement of CMC's.

Many physical quantities plotted against concentration may be used to determine CMC's, a sudden change in which usually signifies the presence of micellar aggregates. Electrical conductivity was used in this work as a convenient means of determining the CMC and the fraction of bound ions.

The specific conductivity of a solution of CsPFO at concentration c above the CMC = c_0 may be regarded as having contributions from three components i.e. those due to dissociated CsPFO at the CMC, micellar ions and excess unbound counterions.

The specific conductivity κ at concentration c may be written[39]

$$1000\kappa = c_0(\Lambda_{Cs^+} + \Lambda_{PFO^-}) + \frac{c-c_0}{N}\Lambda_{mic} + (c-c_0)\frac{z}{N}\Lambda_{Cs^+} \qquad 5.5$$

where Λ_{Cs^+}, Λ_{PFO^-}, and Λ_{mic} are the equivalent molar conductivities of Cs^+, PFO^-, and micellar ions. Below the CMC, only the first term on the right hand side of equation 5.5 contributes to κ. Above the CMC κ is also dependent on micellar contributions and those from unbound Cs^+ ions (the last two terms in equation 5.5) hence there is a break in the κ vs c curve at the CMC. The fraction of *unbound* Cs^+ ions $\alpha \equiv z/N = (1-\beta)$ may be obtained from the ratio of the κ *vs* c slopes above and below the CMC[40,41].

Thus the necessary parameters required to calculate ΔG° can be extracted from the CMC plots of conductivity *vs* concentration.

5.3. CMC Results.

The concentration dependence of the conductivities κ in CsPFO/amide/D_2O solutions at 298 K are presented in figure 5.2. As mentioned in chapter 2, samples were prepared such that the mole fraction of amide in D_2O was 0.00231 (corresponding to approximately 5% by mass FA in D_2O). CMC results extracted from these plots are tabulated in table 5.1. Clear trends in these results are

(i) a montonic increase in the fraction of free counterions with added amide,

(ii) decreasing cmc in the order FA>D_2O>NMF>DMF>DMA, and

(iii) decreasing standard molar free energy of micellisation with added amide.

It is interesting to note that the increasingly positive ΔG° is at odds with a decreasing CMC which can be attributed to the marked effect the presence of amide has on counterion dissociation. Interpretation of these trends will follow in the discussion.

Table 5.1 CMC Results Summary

	α	$\frac{\Delta G^{\circ}}{RT}$	CMC mole fraction /1000
CsPFO/D_2O	0.32	-12.76	0.502
CsPFO/D_2O/FA	0.40	-12.02	0.547
CsPFO/D_2O/NMF	0.57	-11.00	0.457
CsPFO/D_2O/DMF	0.61	-11.20	0.317
CsPFO/D_2O/DMA	0.66	-10.95	0.282
CsPFO/D_2O/NMF x2	0.65	-10.33	0.476

Figure 5.1 (a) Concentration dependence of the conductivities κ in CsPFO/FA/D_2O, CsPFO/NMF/D_2O and CsPFO/DMF/D_2O solutions at 298 K. The mole fraction of amide in D_2O was constant at 0.0231 (corresponding to approximately 5% by mass FA). CMC's were determined from the intersection of the best fit lines above and below the breakpoint in slopes. Plots are divided between two graphs for clarity and to illustrate extrema in slope difference (graph (b)).

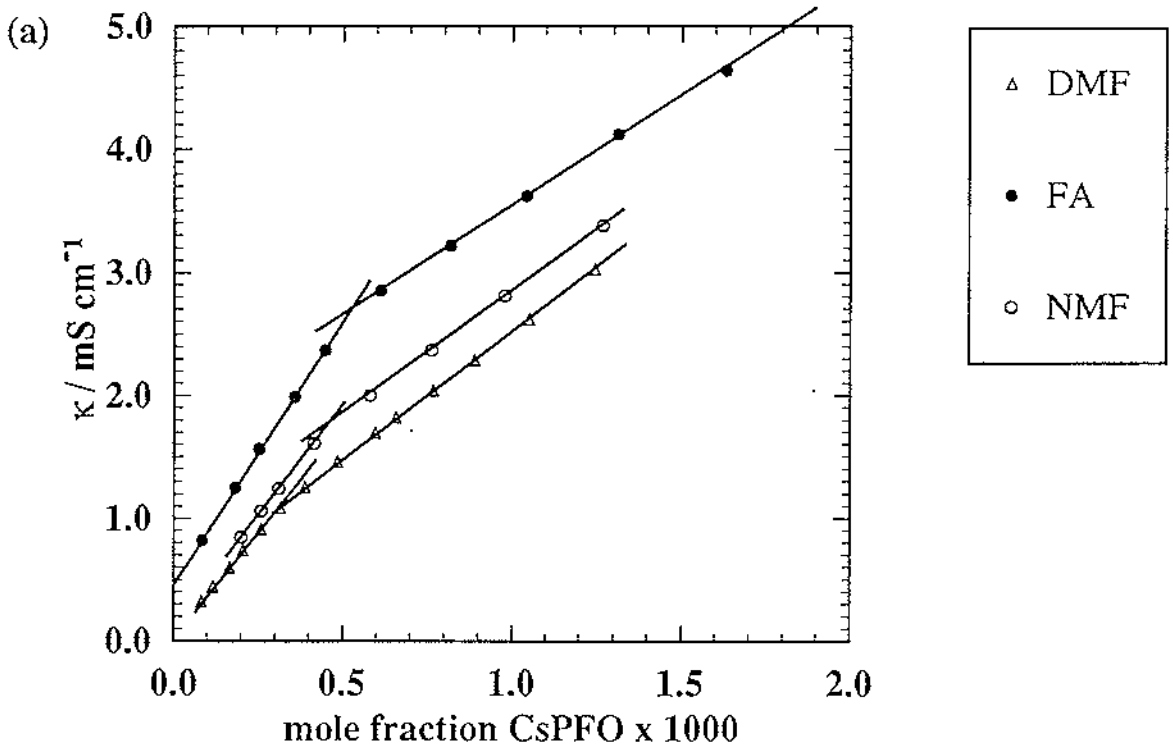

Figure 5.1 (b) Concentration dependence of the conductivities κ in CsPFO/D_2O and CsPFO/DMA/D_2O solutions at 298 K. The mole fraction of DMA in D_2O was constant at 0.0231 (corresponding to approximately 5% by mass FA). CMC's were determined from the intersection of the best fit lines above and below the breakpoint in slopes.

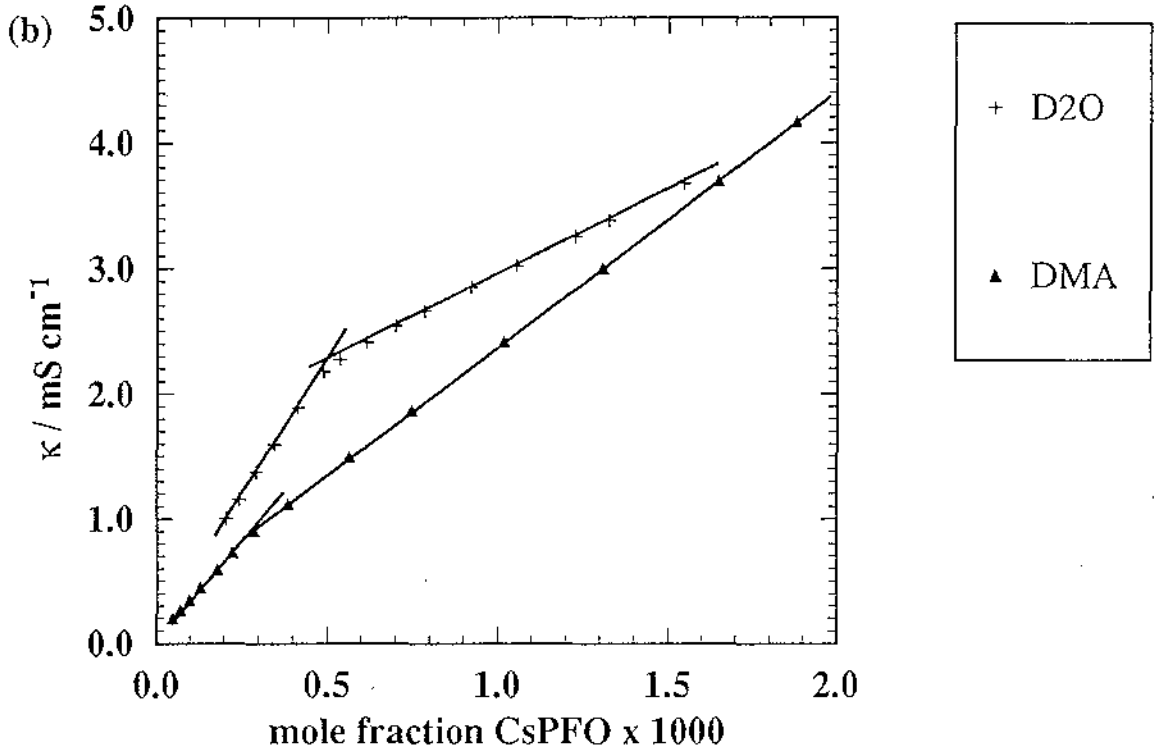

6. Discussion.

6.1. Nature of I/N and N/L transitions in the binary systems.

Previous x-ray work on the CsPFO/D_2O[42] and APFO/D_2O[43] have established that at a given volume fraction the micelles have the same a/b ratio in both systems. In addition at T_{NI} the actual a/b vs ϕ dependence[31] is close to that predicted by a hard particle model[18]. Recent work on the Cs salts of perfluorinated carboxylic acids of chain lengths C_7 to C_{10} have shown that the phase behaviour along T_{NI} is also determined by hard particle interactions[44]. The parallel behaviour established along T_{IN} and T_{LN} in all the systems studied suggests that the driving force for the lamellar-to-nematic transition is the same as that for the nematic-to-isotropic transition.

For all the solvent systems studied here the ^2H NMR measurements show that the hard particle model applies, i.e. at both the nematic-to-isotropic and the lamellar-to-nematic transitions, the transitions occur when the micelles attain a certain a/b ratio, which is the same as that for the binary w=0.5 CsPFO/D_2O system. Thus, in the ternary system also, the mechanism for the phase transition is a hard particle one. The ^2H quadrupole splittings presented in section 4.3 show that the addition of co-solvent produces smaller micelles and since the micelle sizes are the same at the transitions these decrease as the co-solvent concentration increases - decrease in temperature causes an increase in micelle size. Thus, in order to understand the phase behaviour it is necessary to consider the effects of co-solvent on the self-assembly of the micelles.

6.2. Self Assembly of the Micelles in the Ternary Systems.

These will be considered in the context of the McMullen[7,8] model for self assembly. The chemical potential for a surfactant in environment i (body or rim) with head group area a, can be written

$$\tilde{\mu}_i^o(a) = h_i(a) + g_i(a) \qquad (6.1)$$

where $h_i(a)$ represents contributions from interfacial free energy (γa) and electrostatic repulsion (c/a), and $g_i(a)$ represents the 'bulk' free energy associated with packing of hydrophobic chains in the micelle. The latter depends not only on the head group area, but also on the compressional and splay elasticity of the chains, which is dependent on the thickness and curvature of the surfactant "film". The average chemical potential of a surfactant in an aggregate consisting of n surfactants will, therefore, depend in a

complicated way on the number of molecules in the 'rim' with respect to the 'body' so that equation 6.1 can be written[7]

$$\tilde{\mu}_n^o = \tilde{\mu}_{\infty b}^o + f(n)\alpha(n)kT \qquad (6.2)$$

where the fraction of surfactants in the rim $f(n)$ and the difference in the chemical potentials in the rim and the body $\alpha(n)kT$ are both complex functions of n and the latter quantity is also a function of the average a_o of the optimum head group areas $a_o^{(i)}$ in the body and rim. By this model, providing the molecular interactions are such as to make $\alpha(n)$ very small, then micelles with small n will be thermodynamically stable.

The micelle size distribution is given by

$$x_n = n x_1^n \exp\left[n\left(\mu_1^0 - \tilde{\mu}_n^0\right)/kT \right] \qquad (6.3)$$

where x_n is the mole fraction of surfactant n-mers, and x_1 and μ_1^0 are respectively, the mole fraction and the chemical potential of the monomers. Equation 6.3 is identical to equation 5.4. It has been shown[2] that, with all other things being equal, a decrease in $\tilde{\mu}_n^0$ is associated with a shift in the distribution towards a larger micelle.

Effect of Temperature on the Self Assembly.

The NMR measurements show that the effect of decreasing temperature is to shift the distribution of micelle sizes to higher aggregation number i.e. they get bigger. The primitive micelle structure of the Taylor/Herzfeld[18] model explains the observed temperature dependence of micelle size by a decrease in free energy of association per monomer-monomer contact ($-\phi(T)k_BT$) with increase in temperature, i.e. ϕ decreases in an approximately linear manner with T^{-1}. It is not clear what the predicted temperature dependence will be in the McMullen model. On the one hand the increase in the splay elasticity (increase in $g_{II}(a)$) with increasing temperature would, in the absence of any redistribution of the fraction of surfactants in the rim ($f(n)$), leads to smaller micelles. On the other hand, however, the free energy could be minimised in response to this by creating more body (decreasing$f(n)$). An alternative mechanism by means of which the decrease in micelle size with increasing temperature may be explained, and one that has successfully explained the isotope effect in CsPFO/water systems[1], is that the origin of the micelle size decrease with increasing temperature is most likely the effect of temperature on the binding of the ions at the surface of the micelle. The isotope effect on the phase behaviour of the CsPFO/water system on substituting water for heavy water has been attributed to tighter binding of Cs^+ ions to surface carboxylate groups *via* bridging water molecules in the case of D_2O[2]. The micelle size decreases as the

temperature is raised is similarly accounted for in terms of bonding through a bridging water molecule. On raising the temperature, the hydrogen-bond will weaken, that is, the CO_2^--Cs^+ distance will increase and the screening of the repulsive force will be reduced. Thus, a_0 will increase and there will be a corresponding decrease in micelle size. The presence of co-solvent will moderate this interaction to some degree but in this work, since the co-solvent mole fraction is very much less than that of the D_2O, it is expected to be a small effect.

Effect of Co-solvent on the Self Assembly.

The effect of adding co-solvent to the CsPFO/D_2O system at constant temperature is to shift the equilibrium of micelle sizes to lower aggregation number i.e. they get smaller, and the order of effects is FA<<NMF<DMF<DMA. This may be explained in terms of changes in $h_i(a)$ since there is no reason to suspect any direct changes in the configurational entropy of the fluorocarbon chains upon introducing amide molecules to the system. Thus, while changes in $h_i(a)$ may lead to changes in $g_i(a)$, the latter will be an "effect" rather than a "cause" of the change.

One effect of adding these particular amides to the system is to alter the relative permittivity ε_r of the solvent medium. A decrease in ε_r serves to increase the c/a term leading to smaller micelles. However, since the ε_r values of the pure amides (see table 6.1) reflect their effect on the ε_r of water[45-47], it is clear that changes in the solvent bulk relative permittivity cannot be the cause of the observed phase behaviour (changes in micelle size). If they were, the addition of NMF and FA would result in micelle growth (i.e. increase the phase transition temperatures) whereas the opposite is observed. Thus changes in relative permittivity are not responsible for the observed universal decrease in micelle sizes.

The amides will also change the surface tension γ. A decrease in γ leads to a decrease in micelle size through the γa term of $h_i(a)$ in equation 6.1. This is an attractive term and so a decrease in this will result in a more positive $\tilde{\mu}_i^o(a)$ i.e. a smaller micelle. The surface tensions of the pure solvents do reflect the order of the amides' effects on micelle size (table 6.1) and this provides a possible explanantion for changes in the phase transition temperatures. However, the behaviour of mixed solvents becomes complex in the presence of solutes (i.e Cs^+ and PFO^- ions) and it is most often found that components of binary solvent mixtures exhibit some 'heteroselectivity' or 'preferential solvation' toward solutes which would tend to negate bulk properties of pure solvent mixtures.

Table 6.1 Relative Permittivities (298 K) and Surface Tensions (303 K).

	^2H_2O	FA	NMF	DMF	DMA
ε_r	78.3	111.3	185.5	36.7	37.8
γ / mJm^{-2}	70.1	56.6	38.0	35.6	32.4

The phenomenon of preferential solvation of ions in aqueous mixtures of these solvents has been extensively studied. NMR relaxation measurements[48-51] showed that the preference of the amides for anions in water-rich mixtures occurs in the order DMA>DMF>NMF whilst no specific preference for anions was shown in the case of FA.

That there is a surface-specific interaction of the amide with the PFO^- micelle is clear from the results of measurements made on the system CsPFO/D_2O/DMF-d_7. A sample with a constant CsPFO to ^2H_2O mass ratio of 1:1 and a mole fraction of DMF-d_7 of 0.0174 was prepared and the ^2H spectrum obtained in both the isotropic and lamellar phases. The spectrum in the isotropic phase consists of a singlet and a nearly symmetric doublet each of intensity three times that of the singlet, hence the former is from the CDO deuteron and the latter from the CD_3 groups. It is possible to resolve signals from the non-identical CD_3 groups because exchange between sites is slow on the NMR time scale at the experimental temperatures, as a consequence of the partial double bond character of the C-N bond. The inner peak of the doublet can be assigned to the CD_3 group *cis* to the CDO deuteron since this is broader due to scalar coupling with that deuteron.

In both the nematic and lamellar phases, these peaks are split into doublets possessing a complex fine structure due to dipole-dipole couplings as shown in figure 6.1 which is a lamellar phase spectrum. The outer doublet of the spectrum is readily assigned to the CDO deuteron on intensity grounds but the origin of the two inner doublets is not clear. It is interesting to compare the magnitudes of the quadrupole coupling constants observed here with those for the DMF-d_7 molecule aligned in the nematic phase of a thermotropic liquid crystal[52]. In the thermotropic solvent these are 11.4, 5.3 and 2.7 kHz compared to 10.1, 6.0 and 4.2 kHz splittings in figure 6.1. These latter splittings vary with $\langle P_2 \cos\alpha \rangle_S$ but this variation is small compared to the total magnitude. In addition the order parameter of the two systems (thermotropic and lyotropic) will be of similar magnitude. The important point is that the ratios of the splittings in the two environments are different. It is the *intra*molecular electric field gradient which determines the value of the quadrupole splittings in the DMF-d_7 molecule[52]. The change in the quadrupole splitting ratios imply a polarization of the

bonding electrons in DMF-d_7 due to a strong amide-PFO^- interaction at the micelle surface through hydrogen bonding[53-55] between the carboxylate head group and the CDO deuteron. In view of this strong surface interaction, the observed co-solvent effects can be understood in terms of their effects on the Cs^+ ion binding to the micelle surface. The CMC measurements reveal a decrease in β for the amide/water systems which is in the same order as their effects on phase transition temperatures, i.e the smaller β, the larger the reduction in the phase transition temperature. The same order in the β value is also observed in the ^{133}Cs isotropic shift measurements of section 4.3.5. A decrease in β will cause an enhancement in the electrostatic repulsion between neighbouring head groups at the micelle surface and this will lead to an increase in the chemical potential of surfactant in the micelle through the *c/a* term in equation 6.1, and consequently smaller micelles will result[7,8]. It is not clear what causes Cs^+ ions to "unbind" from the surface in the presence of amides. It could be a simple steric effect or there could be unfavourable Cs^+-amide interactions which would push the Cs^+ ions away from the surface. Aqueous mixtures of polar molecules with more than one methyl group possess structural peculiarities which influence their selective solvation behaviour[49,50]. In water rich mixtures these solvents are themselves strongly hydrophobically hydrated. Methyl groups may be considered 'dielectric holes' because the volume filled by the CH_3 group can never assume an appreciable amount of electric polarisation[56]. In solvents with high dipole moments, such as those under consideration (see table 6.2), these dielectric holes produce strong electric field gradients directing the water molecules - possibly through interaction with the water quadrupole moment such that the negative ends of the water molecules have a preferred orientation toward the dielectric hole and the positive ends toward the bulk. This has been shown experimentally[56]. It is feasible then that anions have an additional attraction via the directed water molecules, whereas cations are repelled or the cations influence the water molecules in such a way that the special arrangement of water near hydrophobic groups is destroyed when a cation is in the neighbourhood.

Table 6.2 Dipole Moments.

	H_2O	FA	NMF	DMF	DMA
μ / D	1.84	3.68	3.86	3.90	3.79

6.3 Conclusions.

- The phase transitions in the CsPFO/D_2O/co-solvent systems studied here have been shown to be dominated by hard particle interactions.

- The phase behaviour is thus understood in terms of the micelle self assembly.

- Micelle self assembly is affected by the co-solvent so as to produce smaller micelles in all cases and in order to recover the appropriate micelle size at the transition the temperature must be decreased.

- The observed depressions in the phase transition temperatures are in the same order as the reduction in the fraction of Cs^+ ions bound to the micelle surface.

- Both the temperature dependence and the co-solvent dependence are explained in terms of Cs^+-surface interactions.

Figure 6.1 ^2H spectrum of a sample with a constant CsPFO to ^2H_2O mass ratio of 1:1 and a mole fraction of DMF-d_7 of 0.0174 at 278.20 K in the lamellar phase. The outer doublet is attributable to the DMF-d_7 CDO deuteron, the next two extreme doublets to the CD_3 groups and the inner doublet to ^2H_2O. Fine structure in the DMF-d_7 signals is due to dipole-dipole coupling. As an indication of the relative intensities of the ^2H_2O and DMF-d_7 ^2H signals this spectrum has a y-gain of 500 whereas a y-gain of 3 is enough for the ^2H_2O signal to have a similar intensity.

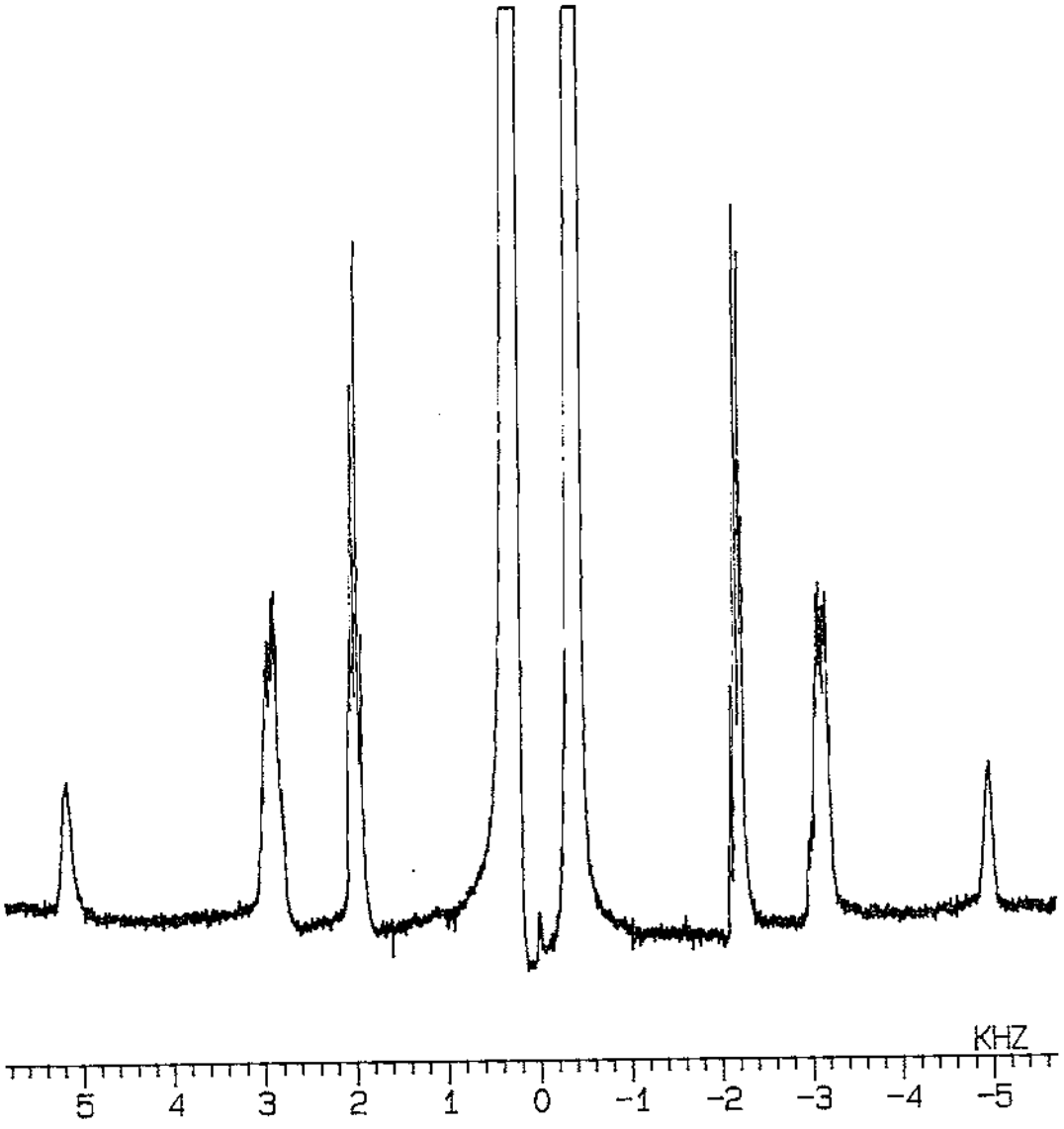

Appendix 1. Phase Transition Temperatures.

Table A1.1 Phase transition temperatures for samples with constant CsPFO:D_2O mass ratio of 2:3 and a DMF mole fraction of x.

x	T_{IN} / K	T_{NI} / K	T_{LN} / K
0.00000	306.713	306.502	301.488
0.00041	306.321	306.091	300.710
0.00117	304.950	304.719	299.597
0.00238	302.903	302.670	297.212
0.00412	299.130	298.903	293.102

Table A1.2 Phase transition temperatures for samples with constant CsPFO:D_2O mass ratio of 1:1 and a co-solvent mole fraction of x.

	x	T_{IN} / K	T_{NI} / K	T_{NL} / K	T_{LN} / K
FA	0.00000	320.323	319.816	315.329	315.089
	0.00491	317.926	317.547	312.391	312.147
	0.01142	314.000	313.400	307.933	307.693
	0.01489	311.609	311.101	305.536	305.298
NMF	0.00533	314.174	313.293	307.740	307.501
	0.00954	307.096	306.427	299.943	299.707
	0.01224	302.679	302.291	295.764	295.527
DMF	0.00255	318.376	317.851	312.855	312.619
	0.00444	316.183	315.688	310.193	309.954
	0.00653	312.481	311.929	306.348	306.107
	0.00808	308.994	308.361	303.048	302.805
	0.01710	290.008	289.586	282.782	282.581
DMA	0.00532	313.340	312.755	307.779	307.536
	0.01297	294.214	293.246	286.135	285.883

Appendix 2 Hazard Sheet.

Chemical	Flash Point / °C	Hazard	Precautions
HPFO	-	Irritant. May be harmful by ingestion, inhalation and skin absorption.	Gloves.
$CsCO_3$	-	May be harmful by ingestion, inhalation and skin absorption.	Gloves.
CsPFO	-	unknown.	Gloves.
D_2O	-	May be harmful by ingestion, inhalation and skin absorption.	Gloves.
n-Butanol	35	May be harmful by ingestion, inhalation and skin absorption. Flammable.	Gloves. Fume cupboard. Avoid naked flames and strong heat.
Hexane	-23	Irritant. May be harmful by ingestion, inhalation and skin absorption. Flammable.	Gloves. Fume cupboard. Avoid naked flames and strong heat.
FA	154	Teratogenic. Could produce defects in unborn children. Irritant. May be harmful by ingestion, inhalation and skin absorption. Flammable.	Gloves. Fume cupboard. Avoid naked flames and strong heat.
NMF	98	as for FA.	as for FA.
DMF	57	as for FA.	as for FA.
DMA	70	as for FA.	as for FA.
DMF-d_7	57	as for FA.	as for FA.

References.

(1) Boden, N.; Corne, S. A.; Jolley, K. W. *J. Phys. Chem.* **1987**, *91*, 4092-4105.

(2) Boden, N.; Jolley, K. W.; Smith, M. *Journal of Physical Chemistry* **1993**, *97*, 7678-7690.

(3) Boden, N.; Clements, J.; Jolley, K. W.; Parker, D.; Smith, M. H. *J. Chem. Phys.* **1990**, *93*, 9096-9105.

(4) Boden, N.; Corne, S. A.; Holmes, M. C.; Jackson, P. H.; Parker, D.; Jolley, K. W. *J. Physique* **1986**, *47*, 2135-2144.

(5) Holmes, M. C.; Reynolds, D. J.; Boden, N. *J. Phys. Chem.* **1987**, *91*, 5257-5262.

(6) Israelachvili, J. N.; Mitchell, D. J.; Ninham, B. W. *J. Chem. Soc. Faraday Trans. I* **1976**, *72*, 1525-1568.

(7) McMullen, W. E.; Ben-Shaul, A.; Gelbart, W. M. *J. Colloid Interface Sci.* **1984**, *98*, 523-536.

(8) McMullen, W. E.; Gelbart, W. M.; Ben-Shaul, A. *J. Phys. Chem.* **1984**, *88*, 6649-6654.

(9) Onsager, L. *Ann. N. Y. Acad. Sci.* **1949**, *51*, 627-659.

(10) Frenkel, D.; Eppenga, R. *Mol. Phys.* **1984**, *52*, 1303.

(11) Frenkel, D.; Eppenga, R. *Phys. Rev. Lett.* **1982**, *49*, 1089-1092.

(12) Frenkel, D.; Mulder, B. M.; McTague, J. P. *Phys. Rev. Lett.* **1984**, *52*, 287-290.

(13) Frenkel, D.; Mulder, B. M. *Mol. Phys.* **1985**, *55*, 1171.

(14) Allen, M. P.; Wilson, R. W. *Journal of Computer-Aided Molecular Design* **1989**, *3*, 335 - 353.

(15) Tjipto-Margo, B.; Evans, G. T. *J. Chem. Phys.* **1990**, *93*, 4254.

(16) Allen, M. P.; Frenkel, D.; Talbot, J. *J. Comput. Phys. Rep.* **1989**, *9*, 301.

(17) Sluckin, T. J. *Liq. Cryst.* **1989**, *6*, 111.

(18) Taylor, M. P.; Herzfeld, J. *Physical Review A* **1991**, *43*, 1892-1905.

(19) Boden, N.; Jolley, K. W.; Smith, M. H. *Liq. Cryst.* **1989**, *6*, 481-488.

(20) Rosenblatt, C. *J. Phys. Chem.* **1987**, *91*, 3830-3834.

(21) Rosenblatt, C.; Zolty, N. *J. Physique Lett.* **1985**, *46*, L-1191-L-1191.

(22) Parbhu, A. N. Master of Science Thesis, Massey University, 1990.

(23) Boden, N.; Corne, S. A.; Halford-Maw, P.; Fogarty, D.; Jolley, K. W. J. *J. Magn. Res.* **1992**, *98*, 92.

(24) Abragam, A. *The Principles of Nuclear Magnetism*; Oxford University Press: Oxford, 1961.

(25) Pake, G. E. *Solid State Phys.* **1956**, *2*,

(26) Cohen, M. H.; Reif, F. *Solid State Physics* **1957**, *5*, 321-395.

(27) Boden, N.; Jones, S. A. *N.A.T.O. ASI. Sci. C. Maths. Phys.* **1985**, *141*, 437.

(28) Saupe, A. Z. *Naturforsch* **1964**, *19a*, 161.
(29) Persson, N.-O.; B., L. *J. Phys. Chem.* **1979**, *83*, 3015-3019.
(30) Dietrich, R.; Trahms, L. *J. Magn Reson.* **1987**, *71*, 337-341.
(31) Boden, N.; Edwards, P. J. B.; Jolley, K. W. In *Structure and Dynamics of Strongly Interacting Colloids and Supramolecular Aggregates in Solution*; S.-H. Chen, J. S. Huang and P. Tartaglia, Ed.; Kluwer academic Publishers: Dordrecht, 1992; Vol. 369; pp 433-461.
(32) Boden, N.; Hedwig, G. R.; Holmes, M. C.; Jolley, K. W.; Parker, D. *Liq. Crystals* **1992**,
(33) Jolley, K. W.; Smith, M. H.; Boden, N. *Chem. Phys Lett.* **1989**, *162*, 152-156.
(34) Sandstrom, J. *Dynamic NMR Spectroscopy*; Academic: New York, 1982.
(35) Taylor, M. P.; Herzfeld, J. *J. Phys.: Condens. Matter* **1993**, *5*, 2651-2678.
(36) Lindblom, G.; Wennerström, H.; Lindman, B. *Chem. Phys. Lett.* **1971**, *8*, 489.
(37) Berr, S. S.; Coleman, M. J.; Jones, R. R. M.; Johnson, J. S., Jr *J. Phys. Chem.* **1986**, *90*, 6492-6499.
(38) Israelachvili, J. N.; Mitchell, D. J.; Ninham, B. W. In *Faraday Trans. II*; 1976; pp 1525-1568.
(39) Evans, H. C. *J. Chem. Soc.* **1956**, 579-586.
(40) Evans, D. F.; Wightman, P. J. *J. Colloid Interface Sci.* **1982**, *86*, 515-524.
(41) Evans, D. F.; Allen, M.; Ninham, B. W.; Fouda, A. *J. Solution Chem.* **1984**, *13*, 87-101.
(42) Holmes, M. C.; Charvolin, J.; J., R. D. *Liq. Cryst.* **1988**, *3*, 1147-1155.
(43) Clements, J. *Personal Communication.*
(44) Parbhu, A. N. *Ph.D thesis work*, to be published 1994.
(45) Kumbharkhane, A. C.; Puranik, S. M.; Mehrotra, S. C. *J. Solution Chem.* **1993**, *22*, 219-229.
(46) Douzou, P. *Cryobiochemistry An Introduction*; Academic Press: London, 1977.
(47) Rohdewald, P.; Moldner, M. *J. Phys. Chem.* **1973**, *77*, 373-377.
(48) Holz, M.; Rau, C. K. (. F. *J. Chem. Soc., Faraday Trans. I* **1982**, *78*, 1899-1910.
(49) Holz, M.; Sacco, A.; Trotta, M. *J. Solution Chem.* **1990**, *19*, 193-205.
(50) Holz, M.; Weingartner, H.; Hertz, H. G. *J. Solution Chem.* **1978**, *7*, 705-720.
(51) Holz, M. *J. Chem. Soc., Faraday Trans. I* **1977**, *74*, 644-656.
(52) Balakrishnan, N. *J. Magn. Res.* **1989**, *83*, 233-245.
(53) Finter, C. K.; Hertz, H. G. *Zeitschrift fur Physikalische Chemie Neue Folge* **1986**, *148*, 75-96.
(54) Finter, C. K.; Hertz, H. G. *J. Chem. Soc., Faraday Trans. I* **1988**, *84*, 2735-2754.
(55) Finter, C. K.; Hertz, H. G. *J. Chim. Phys.* **1988**, *85*, 589-596.
(56) Hertz, H. G.; Holz, M. *J. Phys. Chem.* **1974**, *78*, 1002-1013.